On denoising images using wavelet-based statistical techniques

Imola K. Fodor and Chandrika Kamath

`fodor1@llnl.gov` and `kamath2@llnl.gov`

Center for Applied Scientific Computing

Lawrence Livermore National Laboratory

P.O. Box 808, Livermore, CA 94551

Abstract—

Techniques based on thresholding of wavelet coefficients are gaining popularity as approaches to denoising data. The main idea is to transform the data into a different basis, the wavelet basis, where the "large" coefficients are mainly the signal, and the "smaller" ones represent the noise. By suitably modifying the coefficients in the new basis, the noise can be removed from the data. Much of the work done in this field has focused on one dimensional data, though a few publications have compared select two-dimensional generalizations. In this paper, we extend several one-dimensional denoising procedures to two dimensions, and provide a comprehensive evaluation of the resulting methods. We show that for images, there are several different ways in which these techniques can be applied. Using test images corrupted by additive Gaussian noise, we compare and contrast the methods across a range of noise levels. Our results, using the mean squared error as a measure of the quality of denoising, show that the *SureShrink* and the *BayesShrink* methods consistently outperform the other wavelet-based techniques we considered. We also compare the effectiveness of these methods with simple spatial filters. While no filter was consistently the best, we found that a combination of the minimum mean squared error filter, followed by a Gaussian filter, often led to smaller error than the best wavelet techniques.

I. Introduction

With sensors becoming ubiquitous and computers becoming more powerful, scientists are collecting and analyzing data at an ever increasing pace. This has resulted in several interesting problems in the analysis of data from areas as diverse as astronomy, medical imaging, and computer vision. In these fields, the data that is collected by sensors is often noisy, either as a result of the data acquisition process or due to natural phenomena such as atmospheric disturbances. Therefore, removing the noise from the data is an important problem that must be addressed before we can analyze the data.

One approach to denoising data, proposed by several researchers in the statistics and signal processing communities, involves the thresholding of wavelet coefficients, as described in [31], [13], [14], [15], [2], [20], [30], and the references therein. Most methods in the literature have been designed for one-dimensional signals, but they can be easily extended to higher dimensional signals as well. More recent publications dealing directly with images include [10], [9], [6], [25].

In this paper, we compare and contrast various wavelet denoising techniques that have been proposed in the literature using two-dimensional data as an example. This work was done as part of the Sapphire project in large-scale scientific data mining [22], which involves the analysis of massive data sets arising in scientific applications. As these data are frequently noisy, with the noise statistics varying from domain to domain, and sometimes from image to image, we developed a software toolkit to enable experimentation with the different options in wavelet denoising. Our goal was three-fold. The first was to create a comprehensive software library of wavelet denoising techniques to complement the extensive literature on the subject. While there are some software packages such as MR/1 [21] that include denoising using wavelets, none provide a complete implementation of all the techniques proposed in the literature. Second, we wanted to provide scientists, who are not experts in wavelet denoising, with a choice of techniques, so that they could select a combination appropriate for their data. Third, we wanted to compare and contrast the various options in order to provide guidance and recommendations on their usage.

This paper is organized as follows. Section II provides a brief introduction to the technique of denoising by thresholding of wavelet coefficients. We explain the various options in the denoising methods such as the choice of wavelet transforms, noise estimation techniques, threshold calculation methods (or shrinkage rules), and threshold application schemes (or shrinkage functions). Next, in Section III, we provide a comprehensive evaluation of the various methods. We compare the performance of various denoising combinations on test images with simulated noise and evaluate them with respect to the known noiseless images. In Section IV, we compare and contrast these wavelet-based techniques with the more traditional approaches to denoising based on spatial filters. Finally, in Section V we summarize our findings and propose ideas for future work.

II. Wavelet denoising

The problem of denoising data can be stated as follows: given the zero-mean observation data $Y_{i,j}$ as a noisy realization of the signal $X_{i,j}$:

$$Y_{i,j} = X_{i,j} + \epsilon_{i,j}, \quad i = 1, \cdots, I, \quad j = 1, \cdots, J, \qquad (1)$$

find an "optimal" estimate of $X_{i,j}$ based on $Y_{i,j}$. The solution to this optimization problem depends on the distribution of the noise $\{\epsilon_{i,j}\}$ and on the form of the optimization criterion. A common approach, assumed throughout this paper, is to specify that the $\{\epsilon_{i,j}\}$s are independent from the signal and are independent and identically distributed (*iid*) Gaussian random variables, $\epsilon_{i,j} \sim \mathcal{N}(0, \sigma^2)$, and to use the minimal mean square error (MSE) to evaluate the optimality of the estimates. Though we stated the problem using two-dimensional data as an example, it can be applied to data in any number of dimensions.

Wavelet denoising provides one particular way of obtaining the estimates $\hat{X}_{i,j}$ of the original signal $X_{i,j}$. The main idea is to transform the data into a different basis, where the "large" coefficients correspond to the signal, while the "small" ones represent mostly the noise in the data. If $\mathbf{Y}$, $\mathbf{X}$, and ϵ denote the observed data, the noiseless data, and the error matrices in Equation (1), respectively, then the three main steps of the wavelet denoising process are as follows:

Step 1. Calculate the wavelet coefficient matrix $\mathbf{w}$ by applying a wavelet transform $\mathbf{W}$ to the data:

$$\mathbf{w} = \mathbf{W}\,\mathbf{Y} = \mathbf{W}\,\mathbf{X} + \mathbf{W}\epsilon, \qquad (2)$$

Step 2. Threshold the detail coefficients of $\mathbf{w}$ to obtain the estimate $\hat{\mathbf{w}}$ of the wavelet coefficients of $\mathbf{X}$:

$$\mathbf{w} \to \hat{\mathbf{w}}, \qquad (3)$$

Fig. 1. Wavelet decomposition subbands using a decimated transform with two multiresolution levels.

Step 3. Inverse transform the thresholded coefficients to obtain the denoised estimate:

$$\hat{\mathbf{X}} = \mathbf{W}^{-1} \, \hat{\mathbf{w}}. \tag{4}$$

Under our assumptions, the orthogonal transform $\mathbf{W}$ in Equation (2) preserves the normality of the errors $\mathbf{W}\epsilon$ in the new wavelet basis. Thus, the wavelet coefficients $w_{i,j}$ of the observed data can be written as noisy realizations of the true wavelet coefficients $\{\mathbf{WX}\}_{i,j} = \mu_{i,j}$ of the unknown signal:

$$w_{i,j} \sim \mathcal{N}(\mu_{i,j}, \sigma^2), \quad i = 1, \cdots, I, \quad j = 1, \cdots, J. \tag{5}$$

The number N of the wavelet coefficients $\mathbf{w}$ in Equation (2) can vary depending on the type of transform used. For example, in the case of decimated transforms [18], [1], there are as many coefficients as the number of points in the dataset. That is, $N = IJ$, regardless of the number of multiresolution levels K used in the decomposition. On the other hand, non-decimated transforms [16], [23], [1], also referred to as stationary or translation-invariant methods, provide an overcomplete representation, resulting in $N = KIJ$ coefficients, with IJ coefficients on each of the K levels. Denoising using the coefficients of the non-decimated transforms generally leads to fewer visual artifacts than denoising based on the corresponding decimated transform [11], [19]. In this paper, we focus on the decimated transforms as they involve fewer coefficients and therefore have lower memory requirements. However, the methods we describe carry over easily to the non-decimated case.

Fig. 1 displays the subbands of a two-level ($K = 2$) decimated decomposition. The N wavelet coefficients are grouped into subbands according to the number of multiresolution levels and three spatial directions (plus the smooth part on the second level). The directions reflect the order in which the high-pass (H) and the low-pass (L) filters corresponding to the wavelet transform are applied along the two dimensions of the original image. First, the original image is decomposed into the level one coefficients, which are represented by the subbands LH_1 (vertical detail, first level), HL_1, (horizontal detail, first level), HH_1 (diagonal detail, first level), and LL_1 (smooth, first level). The smooth part is then similarly decomposed into the four subbands corresponding to the second multiresolution level. The process can be further iterated for additional multiresolution levels. Under this scenario, the number of wavelet coefficients on a given subband at level k is $\frac{I}{2^k}\frac{J}{2^k}$, the number of detail coefficients on level k is $3\frac{I}{2^k}\frac{J}{2^k}$, the number of smooth coefficients

on level k is $\frac{I}{2^k}\frac{J}{2^k}$, and the total number of coefficients on level k is $4\frac{I}{2^k}\frac{J}{2^k}$.

We next provide the details of the three denoising steps in Equations (2)-(4) and the parameters required in each step.

First, we need to select a wavelet for the forward and inverse transformations $\mathbf{W}$ and $\mathbf{W}^{-1}$ in Equation (2) and Equation (4), respectively. We have a choice of either orthogonal or biorthogonal transforms. Well-known orthogonal wavelets include the Haar, the Daubechies family (daublets), the least asymmetric wavelet family (symmlets), and the coiflets [12]. The simplest of the orthogonal wavelets, the Haar wavelet, is symmetric but discontinuous. Its analysis and synthesis filters have a compact support, with two coefficients each. The latter three families of wavelets come in a variety of widths, each associated with a different number of filter coefficients, and possessing different smoothness properties. The daublets are continuous, but asymmetric, with compact support. The symmlets are also continuous with compact support, and are the least asymmetric. In addition to having vanishing moments for the mother wavelets, as the daublets and the symmlets do, the coiflets also have vanishing moments for the father wavelets. The biorthogonal B-spline and V-spline wavelet families are symmetric and, with proper boundary treatments provide perfect reconstruction [12]. It has been argued that the biorthogonal wavelets are preferable over the orthogonal ones as symmetry leads to visually more pleasing results in images [6].

In addition to the choice of a wavelet, we also need to select the number of multiresolution levels in the decomposition, along with the option for handling values near the boundary. We have implemented several boundary treatment rules [29], including periodic, symmetric, reflective, constant, and zero-padding. The periodic extension preserves orthogonality, has perfect reconstruction properties, and can be used for both orthogonal and biorthogonal wavelets. It is therefore the default in most statistical software [2]. For biorthogonal wavelets, the reflection rule preserves biorthogonality, leads to perfect reconstruction, and, in addition, might minimize artifacts at the boundary [2].

Note that for two-dimensional data, it is possible to use a different wavelet in each direction as well as at each level of the multiresolution analysis [27]. We could also use different boundary treatments for each direction at each level.

The last step in the denoising indicated in Equation (4) is straightforward, once the coefficients have been thresholded.

In the remainder of this section, we describe the issues involved in implementing the second step in denoising, namely, the thresholding step in Equation (3). Let w denote a single generic detail coefficient and $\hat{w}$ its thresholded version. Let λ be the threshold, $\delta_\lambda()$ denote the thresholding (or shrinkage) function, and $\hat{\sigma}$ be an estimate of the standard deviation σ of the noise in Equation (1). Then, the thresholded coefficient, $\hat{w}$, is obtained through either

$$\hat{w} = \hat{\sigma} \, \delta_\lambda(w/\hat{\sigma}), \tag{6}$$

or

$$\hat{w} = \delta_\lambda(w), \tag{7}$$

depending on whether the threshold λ was determined assuming a unit noise scale $\sigma = 1$, in which case Equation (6) applies, or an estimation of the actual noise was built-in into the method, in which Equation (7) would be the appropriate choice. Note that, in the notation above, we suppressed the possible dependence of the noise estimate, the threshold, and the thresholding function on either the multiresolution level or the subband.
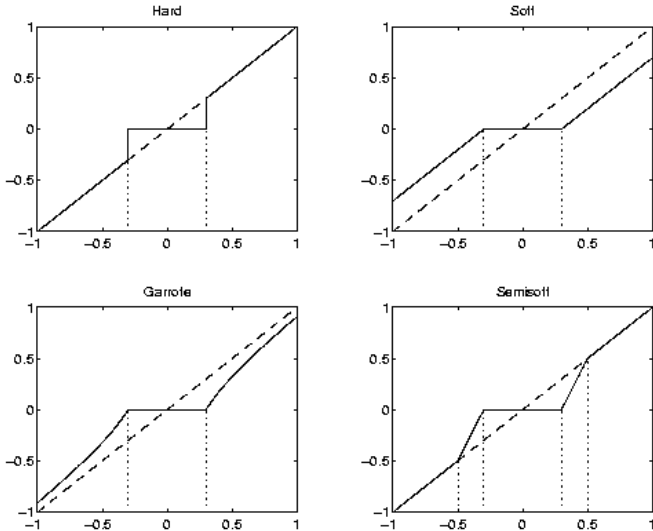
Fig. 2. Thresholding functions.

The various denoising methods we consider differ in the choices for $\delta()$, λ and $\hat{\sigma}$, in Equations (6) and (7). That is, we can obtain different denoisers by considering different

- thresholding or shrinkage functions (Section II-A)
- noise estimates (Section II-B), and
- shrinkage rules to determine the threshold λ (Section II-C).

For one-dimensional data, wavelet denoising methods calculate thresholds either globally, with one threshold for all the coefficients, or on a level-dependent basis, with K different thresholds for the K different dyadic levels. The extension to two dimensions has another possibility - we can calculate thresholds in a subband-dependent manner, that is, $3K$ thresholds for the $3K$ detail coefficient subbands. We found that typical image denoising publications considered either the level-dependent or the subband-dependent alternative in addition to the global implementation [6], [9], instead of including all three possibilities. For the denoising methods considered in our software, we provide all the three different options, namely, global thresholds, level-dependent thresholds, and subband-dependent thresholds.

Next, we describe the different ways in which we can select the thresholding functions, estimate the noise, and select the rules for denoising.

A. Thresholding or Shrinkage Functions

The thresholding or shrinkage function determines how the threshold is to be applied to the data. In this sub-section, we assume that the threshold has already been calculated using one of the rules in Section II-C. Since some of the rules depend on the thresholding function to be applied, the user must first choose the thresholding function.

Fig. 2 displays the four most widely used thresholding functions. The x axis represents the wavelet coefficients w in Equation (2), and the y axis shows the corresponding thresholding function $\delta_\lambda(w)$. We scaled the graphs to the $[-1, 1]$ interval, but the data need not be in that range. The dotted vertical lines indicate the values of the single threshold $\pm\lambda$ for the hard ($\delta_\lambda^H(w)$), soft ($\delta_\lambda^S(w)$) and garrote ($\delta_\lambda^G(w)$) functions. The semisoft function $\delta_{\lambda_1,\lambda_2}^{SS}(w)$ requires two thresholds, $\pm\lambda_1$ and $\pm\lambda_2$, represented by the four dotted vertical lines in its graph.

The hard wavelet shrinkage function depends on a single threshold parameter, and involves a keep or kill strategy. A wavelet coefficient is kept unchanged if it is larger in absolute value than the positive threshold λ, and it is set to zero otherwise:

$$\delta_\lambda^H(w) = wI_{\{|w|>\lambda\}},\qquad(8)$$

where $I_{\{a\}}$ denotes the $\{0, 1\}$ indicator function, corresponding to $\{a = False, a = True\}$.

The soft wavelet shrinkage function also depends on a single threshold value, and is a shrink or kill procedure. A coefficient is shrunk toward zero if its absolute value is larger than the positive threshold, and is set to zero otherwise:

$$\delta_\lambda^S(w) = \text{sgn}(w)(|w| - \lambda)I_{\{|w|>\lambda\}}.\qquad(9)$$

The garrote wavelet shrinkage function also depends on a single threshold value, and is also a shrink or kill procedure. A coefficient is shrunk toward zero if its absolute value is larger than the positive threshold, and is set to zero otherwise:

$$\delta_\lambda^G(w) = \left(w - \frac{\lambda^2}{w}\right)I_{\{|w|>\lambda\}}.\qquad(10)$$

The semisoft shrinkage function is more general than the other shrinkage functions, and includes the hard and the soft functions as special cases. The semisoft function depends on two positive thresholds, λ_1 and λ_2, with $\lambda_1 \leq \lambda_2$. It has the following form:

$$\delta_{\lambda_1,\lambda_2}^{SS}(w) = \left\{\begin{array}{ll} 0, & |w| \leq \lambda_1 \\ \text{sgn}(w)\frac{\lambda_2(|w|-\lambda_1)}{\lambda_2-\lambda_1}, & \lambda_1 < |w| \leq \lambda_2 \\ w, & |w| > \lambda_2. \end{array}\right\}.\qquad(11)$$

B. Noise Estimation Methods

Certain thresholds, as described in Section II-C, are determined assuming a unit noise scale, i.e. $\sigma = 1$. Therefore, in practice, the data must be scaled by $\hat{\sigma}$ according to Equation (6) when applying these thresholds. In some cases, there is prior knowledge about the noise distribution. However, in many situations, $\hat{\sigma}$ must be calculated from the observed data. The options for estimating the noise scale include the choice of the functional form of the estimator and the choice of the detail coefficients to include in the estimation.

We implemented different estimation functions, including the sample standard deviation (sd) and the more robust median absolute deviation (MAD) suggested in [15]. Our software allows the user to calculate noise estimates based on different detail coefficients. For example, global estimates (one estimate for all the coefficients) can be based on either the detail coefficients from a specified level or subband, or all the detail coefficients combined. Level- and subband-dependent estimates (one estimate per level and one estimate per subband, respectively) are calculated using only the coefficients from the corresponding level or subband.

C. Thresholding or Shrinkage Rules

This section describes the options for selecting the thresholds using various thresholding or shrinkage rules. Let λ denote a threshold. For the sake of convenience, the possible dependence of λ on the multiresolution level, $\{k, 1 \leq k \leq K\}$, or on the subband, $\{s, 1 \leq s \leq 3K\}$, is suppressed in the notation.

Certain rules (e.g. *universal*, Section II-C.1) calculate thresholds independently of the shrinkage function, that is, the same threshold is obtained for the soft, hard, and garrote functions. However, other rules (e.g. *SURE*, Section II-C.4) provide

thresholds that depend on the shrinkage function, resulting in different thresholds for the different shrinkage functions. In addition, certain rules assume a unit noise scale for the wavelet coefficients, $\sigma = 1$, others do not. We indicate the assumptions of each method as we describe them in more detail.

C.1 Universal

The *universal* threshold for a signal of size N from a standard normal distribution $\mathcal{N}(0, 1)$ is simply $\lambda = \sqrt{2 \log N}$ [14]. Thus, applying this threshold to the data at hand requires using an estimate $\hat{\sigma}$ in Equation (6). The threshold is determined independently of the shrinkage function. This method was originally proposed as a global thresholding scheme for one-dimensional signals.

C.2 Minimizing the false discovery rate

Thresholds based on minimizing the false discovery rate, *minFDR*, are determined with the aim of minimizing the fraction of coefficients erroneously included in the reconstruction [30]. This method calculates the same threshold for all the shrinkage functions. It was proposed originally as a global thresholding scheme for one-dimensional data. Let Q be the number of coefficients incorrectly kept, and R be the total number of coefficients kept in the reconstruction. Given a predetermined fraction q, the goal is to keep the expected value of Q/R below q. Note that q is similar to the Type I error, usually denoted by α, in testing problems. The calculations proceed as follows. For each of the N wavelet coefficients $w_{i,j}$, first compute the p-values

$$p_{i,j} = 2[1 - \Phi(|w_{i,j}|/\hat{\sigma})], \qquad (12)$$

where $\Phi()$ is the cumulative distribution function of the standard normal distribution $\mathcal{N}(0, 1)$, and $\hat{\sigma}$ is an estimate of the noise standard deviation. Then, order the $p_{i,j}$ values above as

$$p_{(1)} \le p_{(2)} \le \cdots \le p_{(N)}. \qquad (13)$$

Next, starting with $n = 1$, let m be the largest index n such that

$$p_{(n)} \le \frac{n}{N} \, q. \qquad (14)$$

The threshold is then selected as

$$\lambda = \hat{\sigma} \Phi^{-1} \left(1 - \frac{p_{(m)}}{2} \right). \qquad (15)$$

As the estimate of the noise $\hat{\sigma}$ is already factored into the formula, this threshold is applied according to Equation (7).

C.3 Top

The most flexible of all the shrinkage rules, the *top* method requires as input the percentage p of the wavelet coefficients to keep [1]. It does not need to estimate σ as it determines the thresholds directly from the data. Therefore, it is applied to the coefficients using Equation (7). Given p, which is the fraction of the largest coefficients to keep, the threshold λ is simply set to be the $(1-p)$th quantile of the empirical distribution of the absolute values of the wavelet coefficients of interest. The selected threshold does not have any theoretical optimality properties, but it allows the user to experiment with any given dataset by selecting different percentages of the wavelet coefficients to represent the signal. For the semisoft shrinkage function, this method can be called twice, with different parameters, to obtain the lower and the upper thresholds. The threshold is determined independently from the shrinkage function, and was originally proposed as a global method for one-dimensional signals.

C.4 SURE

For one-dimensional data, thresholds derived by minimizing Stein's Unbiased Risk Estimate (*SURE*) depend on the shrinkage function and on the multiresolution level [15]. As mentioned earlier, the generalization to images can be achieved in either level- or subband-dependent manner. In the latter case, the threshold on subband s is

$$\lambda_s = \arg \min_{\lambda \ge 0} \text{SURE}(\lambda, \mathbf{w}_s), \qquad (16)$$

where $\mathbf{w}_s$ denotes the detail coefficients from subband s, and $\text{SURE}(\lambda, \mathbf{w}_s)$ denotes the corresponding Stein's unbiased estimate of the risk corresponding to a specific shrinkage function, as explained in the next paragraphs. The procedure is completely analogous for the level-dependent implementation, except that one changes the subscripts s to l, and substitutes coefficients on a given level $\mathbf{w}_l$ for the coefficients on a given subband $\mathbf{w}_s$ in Equation (16).

Concentrating on the subband-dependent case, for ease of notation, let us rearrange the N_s wavelet coefficients from subband s, $\mathbf{w}_s = \{w_{i,j} : i, j \in$ indices corresponding to subband s$\}$, into the one-dimensional vector $\mathbf{w}_s = \{w_n : n = 1, \cdots, N_s\}$. According to Equation (5), the individual wavelet coefficients $w_{i,j}$ are distributed as $\mathcal{N}(\mu_{i,j}, \sigma^2)$ under our assumptions. Let us next combine the N_s unknown means $\{\mu_{i,j} : i, j \in$ indices corresponding to subband s$\}$ corresponding to the coefficients $\mathbf{w}_s$ from subband s into the corresponding one-dimensional vector $\mu_s = \{\mu_n : n = 1, \cdots, N_s\}$. In vector notation, we have $\mathbf{w}_s \sim \mathcal{N}(\mu_s, \sigma^2)$.

Stein showed that, for almost any fixed estimator $\hat{\mu}_s$ based on the data $\mathbf{w}_s$, the expected loss (i.e. risk)

$$E\{\|\hat{\mu}_s - \mu_s\|_2^2\} \qquad (17)$$

can be estimated unbiasedly. In the general case, assuming $\sigma = 1$, and writing $\hat{\mu}_s = \mathbf{w}_s + \mathbf{g}(\mathbf{w}_s)$, with the $R^{N_s} \to R^{N_s}$ function $\mathbf{g} = \{g_n\}_{n=1}^{N_s}$, we have from [26] that

$$E\{\|\hat{\mu}_s - \mu_s\|_2^2\} = N_s + E\{\|\mathbf{g}(\mathbf{w}_s)\|_2^2 + 2\nabla \cdot \mathbf{g}(\mathbf{w}_s)\}, \qquad (18)$$

where $\nabla \cdot \mathbf{g} \equiv \sum_n \frac{\partial g_n}{\partial w_n}$.

Depending on the estimator $\hat{\mu}_s$, one obtains different formulas for the quantities in Equation (18). For example, in the case of the soft shrinkage function with a fixed threshold λ, we have from Equation (9) that for the nth wavelet coefficient w_n,

$$\hat{\mu}_n^S = \delta_\lambda^S(w_n) = \text{sgn}(w_n)(|w_n| - \lambda)I_{\{|w_n| > \lambda\}}. \qquad (19)$$

Correspondingly,

$$g_n(w_n) = \hat{\mu}_n^S - w_n = \left\{ \begin{array}{ll} -\lambda, & w_n > \lambda \\ -w_n, & -\lambda \le w_n \le \lambda \\ \lambda, & w_n \le -\lambda, \end{array} \right\}, \qquad (20)$$

with

$$\frac{\partial g_n}{\partial w_n} = \left\{ \begin{array}{ll} 0, & w_n > \lambda \\ -1, & -\lambda \le w_n \le \lambda \\ 0, & w_n \le -\lambda, \end{array} \right\}, \qquad (21)$$

$$\nabla \cdot \mathbf{g}(\mathbf{w}_s) = \sum_n \frac{\partial g_n}{\partial w_n} = -\{(\#of \; w_n) : |w_n| \le \lambda\}, \qquad (22)$$

and

$$\|g_n(w_n)\|_2^2 = \left\{ \begin{array}{ll} \lambda^2, & w_n > \lambda \\ w_n^2, & -\lambda \le w_n \le \lambda \\ \lambda^2, & w_n \le -\lambda. \end{array} \right\}. \qquad (23)$$

Equation (23) is equivalent to

$$\|g_n(w_n)\|_2^2 = [\min(|w_n|, \lambda)]^2, \qquad (24)$$

so that

$$\|\mathbf{g}(\mathbf{w}_s)\|_2^2 = \sum_{n=1}^{N_s} \|g_n(w_n)\|_2^2 = \sum_{n=1}^{N_s} [\min(|w_n|, \lambda)]^2. \qquad (25)$$

Substituting all the intermediate results for the data on subband s and the soft shrinkage function into Equation (18), we obtain

$$E\{\|\hat{\mu}_s^S - \mu_s\|_2^2\} = N_s + E\left\{\sum_{n=1}^{N_s}[\min(|w_n|, \lambda)]^2\right\} +$$
$$E\left\{-2[(\#of\ w_n) : |w_n| \le \lambda]\right\}. \qquad (26)$$

The quantity

$$SURE^S(\lambda, \mathbf{w}_s) = N_s + \sum_{n=1}^{N_s}[\min(|w_n|, \lambda)]^2$$
$$-2[(\#of\ w_n) : |w_n| \le \lambda] \qquad (27)$$

therefore, is an unbiased estimate of the risk associated with the soft shrinkage estimator on subband s:

$$E\{\|\hat{\mu}_s^S - \mu_s\|_2^2\} = E\{SURE^S(\lambda, \mathbf{w}_s)\}. \qquad (28)$$

The threshold on subband s to be used with the soft shrinkage function, λ_s^S, is then chosen as the value that minimizes $SURE^S(\lambda, \mathbf{w}_s)$ in Equation (27). Accordingly,

$$\lambda_s^S = \arg\min_{\lambda \ge 0} SURE^S(\lambda, \mathbf{w}_s). \qquad (29)$$

The thresholds above were derived assuming $\sigma = 1$. For data with non-unit variance, the coefficients are standardized by an appropriate $\hat{\sigma}$ estimate before calculating the threshold with Equation (29).

It has been shown that if the wavelet coefficient decomposition is sparse, thresholds based on the SURE method perform poorly. As a solution to the problem, one first tests for "sparseness". If

$$\frac{1}{N_s}\sum_{n=1}^{N_s}\left(\left(\frac{w_n}{\hat{\sigma}}\right)^2 - 1\right) \le \frac{(\log_2 N_s)^{3/2}}{\sqrt{N_s}}, \qquad (30)$$

then one uses the *universal* threshold, otherwise the *SURE* threshold is used for the wavelet coefficients on subband s. This hybrid method, when combined with the soft shrinkage function is referred to as *SureShrink* in the literature.

The level-dependent thresholds corresponding to the soft shrinkage function, λ_l^S, are derived using a formula identical to Equation (29), except that the wavelet coefficients from subband s are replaced by the coefficients from level l:

$$\lambda_l^S = \arg\min_{\lambda \ge 0} SURE^S(\lambda, \mathbf{w}_l). \qquad (31)$$

Thresholds for the other shrinkage functions can be derived following the steps in Equations (19) through (27), starting with the corresponding formula in Equation (19). We worked out the details for hard thresholding, but in reporting the results, we simply call the resulting method *SURE* thresholding with hard function, instead of *WaveChop*, as suggested in [15].

C.5 Hypothesis Testing

The hypothesis testing approach, *hypTest*, for one-dimensional signals calculates level-dependent thresholds based on testing the hypothesis that some of the wavelet coefficients at a given level are zero [20]. In a manner similar to the *SURE* case described in Section II-C.4, thresholds based on hypothesis testing for two-dimensional data can be obtained on either the separate levels or on the separate subbands. However, unlike their *SURE* counterparts, these thresholds are independent of the thresholding function. Using the notation of Section II-C.4 for the subband-dependent version, and assuming that the N_s wavelet coefficients on subband s are normally distributed, i.e. $\mathbf{w}_s \sim \mathcal{N}(\mu_s, \sigma^2)$, one can separate the "large" coefficients from the "small" ones by testing the hypothesis that the mean of some of the wavelet coefficients equals zero. The sequential approach we implemented first finds the largest of the squared wavelet coefficients on the subband, denoted by $w_{(N_s)}^2$, then compares it to the critical value

$$c_{N_s}^\alpha = \left\{\Phi^{-1}\left[\frac{1}{2}((1-\alpha)^{1/N_s} + 1)\right]\right\}^2, \qquad (32)$$

where α is the pre-determined Type I error probability in the testing and $\Phi()$ is the cumulative distribution function of the standard normal density. If

$$\frac{w_{(N_s)}^2}{\hat{\sigma}^2} > c_{N_s}^\alpha, \qquad (33)$$

where $\hat{\sigma}$ is an estimate of the standard deviation of the noise, the null hypothesis of zero mean associated with the largest (in absolute value) coefficient is rejected, and so $w_{(N_s)}$ is retained as signal. The next step in selecting the threshold is to continue the above procedure with the square of the second largest (in absolute value) wavelet coefficient $w_{(N_s-1)}^2$. If $w_{(N_s-1)}^2/\hat{\sigma}^2 > c_{N_s-1}^\alpha$, the procedure continues until at some point the mth largest (in absolute value) coefficient satisfies

$$\frac{w_{(m)}^2}{\hat{\sigma}^2} < c_m^\alpha, \qquad (34)$$

that is, until there is no more significant signal left in the rest of the coefficients. The threshold at subband s is then set as

$$\lambda_s = |w_{(m)}|, \qquad (35)$$

and is applied according to Equation (7).

C.6 BayesShrink

The *BayesShrink* method uses a Bayesian mathematical framework to derive subband-dependent thresholds that are nearly optimal for soft thresholding [9]. The formula for the threshold on a given subband s is:

$$\lambda_s = \frac{\hat{\sigma}^2}{\hat{\sigma}_X}, \qquad (36)$$

where $\hat{\sigma}^2$ is the estimated noise variance, and $\hat{\sigma}_X^2$ is the estimated signal variance on the subband considered. Unless the noise variance is available a-priori, in which case the estimator $\hat{\sigma}^2$ in Equation (36) is replaced by its known value σ^2, it is estimated as the median absolute deviation of the diagonal detail coefficients on level 1 (i.e. subband HH_1). The estimate of the signal standard deviation is

$$\hat{\sigma}_X = \sqrt{\max(\hat{\sigma}_Y^2 - \hat{\sigma}^2, 0)}, \qquad (37)$$

where

$$\hat{\sigma}_Y^2 = \frac{1}{N_s} \sum_{n=1}^{N_s} w_n^2 \qquad (38)$$

is an estimate of the variance of the observations, with N_s being the number of the wavelet coefficients w_n on the subband under consideration. In case $\hat{\sigma}^2 \geq \hat{\sigma}_Y^2$, the threshold is set to $\lambda_s = \max(|w_n|)$, and all coefficients from the subband are set to zero. Since the standard deviation of the noise is already factored in, the thresholds are applied according to Equation (7).

This method has been proposed to be used with soft thresholding. We use the thresholds calculated via this procedure with other thresholding functions as well, but, in compliance with [9], we reserve the term *BayesShrink* for denoising using the soft shrinkage function.

III. RESULTS

This section reports our results on three test images widely used in the image processing community: Lena, Einstein, and Goldhill. For each image, we first obtained a 512×512 noiseless grayscale original. Then, we added Gaussian noise to the images according to Equation (1), using $\sigma = 10, 20$, and 30. Fig. 3 shows the original images, and the noisy version of the Lena image, with $\sigma = 30$. Next, we applied the wavelet denoising methods described in Section II. We evaluated the performances of the methods using the mean square error (MSE) and the signal-to-noise-ratio (SNR) defined below. For a given denoised estimate $\hat{X}(i,j)$ of $X(i,j)$, the MSE is

$$MSE = \frac{1}{IJ} \sum_{i=1}^{I} \sum_{j=1}^{J} (X(i,j) - \hat{X}(i,j))^2, \qquad (39)$$

the corresponding normalized MSE is

$$MSE_n = \frac{\sum_{i=1}^{I} \sum_{j=1}^{J} (X(i,j) - \hat{X}(i,j))^2}{\sum_{i=1}^{I} \sum_{j=1}^{J} X(i,j)^2}, \qquad (40)$$

and the SNR on dB scale [25] is

$$SNR = 10 \, \log_{10} \frac{1}{MSE_n}. \qquad (41)$$

There are other possible choices for evaluating the quality of the results, as there are indications that the MSE does not necessarily correspond to "best" visual quality [6]. Before reporting our main results in Section III-B, we first explain in Section III-A the various choices we made in selecting the parameters for the different denoising methods.

A. Selecting the Parameters for the Methods

This section describes the techniques we employed in selecting the "optimal" parameters used in the various denoising methods. The experiments described in the following paragraphs are all based on the Lena image, with $\sigma = 10$, using the symmlet8 wavelet with four multiresolution levels $(K = 4)$ and periodic boundary treatment. Our choice of the wavelet was prompted by the need for a relatively symmetric wavelet with a reasonably compact support. In each of the following tables, the best parameter set is presented in bold.

For all the methods that required an estimate of σ, we employed the MAD estimator based on the detail coefficients on the HH_1 subband. We experimented with other options as well, but this method, which was suggested in [15], appeared to be indeed the most robust. For example, this method obtains a

q	Global		Subband-dep.		Level-dep.	
	MSE	SNR	MSE	SNR	MSE	SNR
0.01	56.63	16.07	57.98	15.97	57.72	15.99
0.05	44.71	17.09	46.75	16.90	45.08	17.06
0.1	39.84	17.60	41.15	17.46	40.35	17.54
0.2	**36.56**	**17.97**	38.64	17.73	37.32	17.88
0.3	36.96	17.92	38.15	17.78	37.11	17.90
0.4	40.54	17.52	40.48	17.53	40.55	17.52
0.5	45.61	17.01	45.55	17.01	46.03	16.97

p	Global		Subband-dep.	
	MSE	SNR	MSE	SNR
0.05	58.65	15.92	277.02	9.17
0.1	45.67	17.00	204.76	10.49
0.2	37.87	17.82	129.41	12.48
0.3	**36.50**	**17.98**	89.10	14.10
0.4	38.49	17.75	70.24	15.13
0.5	43.07	17.26	59.20	15.87
0.8	71.55	15.05	72.73	14.98

typical estimate of $\hat{\sigma} = 10.52$ for the image with known value of $\sigma = 10$.

For the $minFDR$ method, based on the results of a smaller experiment reported in Table I, we determined the parameter to be $q = 0.2$. As it can be seen in the corresponding columns in Table I, the global implementation outperformed both the level-dependent and the subband-dependent implementations. This agrees with the literature, as this method was proposed for global thresholding. The second best results were obtained with the level-dependent method, while the subband-dependent version lead to the poorest results. In contrast with $q = 0.2$ for the best global implementation, the parameter corresponding to the optimal level- and subband-dependent versions was $q = 0.3$.

Table II presents the first set of findings for the *top* procedure. It compares the global thresholding results with subband-dependent results, using the same fraction p on all the subbands. The difference thus is in the detail coefficients used when calculating the threshold(s): all of them were combined in the former, while only the ones from the given subband were used in the latter. As the rows indicate, the global procedures outperformed the corresponding subband-dependent implementations. This makes sense from a theoretical perspective, as one wishes to keep the largest coefficients overall, not the largest ones from each subband.

Table III presents the results of our next experiment with the *top* method. Because we expected more significant coefficients on the higher multiresolution levels, we varied the parameter p across the different levels, and calculated subband- and level-dependent thresholds. In line with our expectation, we applied more aggressive thresholding on the first level than on the higher multiresolution levels. For the subband-dependent case, we used only the detail coefficients from the given subband in the calculation, while in the level-dependent case we combined all the detail coefficients from a given level. As the bold-face row indicates, the level-dependent implementation with $p_1 = .15$, $p_2 = .4$, $p_3 = .8$, and $p_4 = .95$ outperformed all the subband-

TABLE III

Determining the p parameter for the Top method: subband- and level-dependent thresholds, using different p values on the levels.

	p			Subband-dep.	
level1	level2	level3	level4	MSE	SNR
.1	.2	.8	1	38.08	17.79
.2	.8	.8	.8	38.40	17.76
.15	.4	.8	.9	33.86	18.30
.15	.4	.8	.95	33.86	18.30
.15	.4	.7	.95	34.01	18.28
.15	.3	.9	.95	35.39	18.11
				Level-dependent	
.15	**.4**	**.8**	**.95**	**33.14**	**18.40**

TABLE IV

Determining the α parameter for the HypTest method.

	Global		Subband-dep.		Level-dep.	
α	MSE	SNR	MSE	SNR	MSE	SNR
0.001	93.03	13.91	68.24	15.26	86.79	14.21
0.01	37.23	17.89	37.11	17.90	38.11	17.79
0.05	39.05	17.68	36.07	18.03	36.86	17.93
0.1	38.57	17.74	35.67	18.08	36.37	18.00
0.2	38.05	17.80	35.29	18.12	35.91	18.05
0.3	37.78	17.83	35.08	18.14	35.64	18.08
0.4	37.55	17.85	34.95	18.16	35.46	18.10
0.5	37.39	17.87	34.86	18.17	35.32	18.12
0.9	36.84	17.94	**34.70**	**18.20**	34.88	18.17
0.95	37.75	17.95	34.71	18.19	34.83	18.18
0.99	36.62	17.96	34.79	18.18	34.76	18.19

TABLE V

Determining the p parameters for the global semisoft top combination.

p_1	p_2	MSE	SNR
0.9	0.8	105.41	13.37
0.9	0.1	98.04	13.68
0.5	0.3	90.04	14.05
0.7	0.3	95.74	13.79
0.3	0.1	62.71	15.63
0.7	0.5	101.23	13.55
0.3	0.2	75.90	14.80
0.4	0.2	79.58	14.59
0.15	0.1	56.12	16.11
0.1	0.05	43.64	17.20
0.1	**0.01**	**37.47**	**17.86**
0.05	0.01	44.10	17.15

TABLE VI

Determining the p parameters for the subband-dependent semisoft top combination.

level4	level3	level2	level1	MSE	SNR
.9	.9	.9	.9		
.8	.8	.8	.8	105.41	13.37
.9	.9	.9	.9		
.1	.1	.1	.1	98.08	13.68
.5	.5	.5	.5		
.3	.3	.3	.3	92.75	13.92
.7	.7	.7	.7		
.3	.3	.3	.3	96.16	13.77
.95	.8	.4	.2		
.9	.7	.3	.1	68.63	15.23
.95	.8	.4	.15		
.9	.7	.3	.1	66.66	15.36
.95	.8	.4	.15		
.7	.5	.2	.1	64.84	15.48
.8	.7	.3	.15		
.7	.5	.2	.1	64.36	15.51
.7	**.6**	**.3**	**.15**		
.3	**.2**	**.1**	**.1**	**61.12**	**15.74**
.3	.3	.3	.3		
.1	.1	.1	.1	81.23	14.50
.7	.6	.3	.15		
.1	.1	.1	.1	61.21	15.73

dependent methods, and it even resulted in a superior image than the best image obtained through global thresholding with $p = 0.3$ in Table II. If the noise levels in the three different directions (vertical, horizontal, diagonal) are different across levels, we could also introduce different values for p on the different levels and subbands.

Based on the results summarized in Tables II and III, we set the percentage-to-keep parameter to $p = 0.3$ for the global threshold implementation, and to $p_1 = .15$, $p_2 = .4$, $p_3 = .8$, and $p_4 = .95$ on multiresolution levels one through four, respectively, for the level-dependent pyramidal implementation.

We estimated the best parameter for the *hypTest* approach to be $\alpha = 0.9$ — an unusually high value for a testing problem. However, similarly high values for one-dimensional signals are reported in [3]. Our results are displayed in Table IV. For a fixed value of α, the subband-dependent implementation achieved the lowest, the level-dependent resulted in the second lowest, and the global version lead to the highest MSE value.

For the semisoft thresholding function, we determined two thresholds by using the *top* rule with two different p parameter values. As reported in Table V, the optimal combination for the global implementation was found to be $\{p_1 = 0.1,\ p_2 = 0.01\}$. The results for the subband-dependent method are shown in Table VI. The best subband-dependent result ($MSE = 61.12$) was much worse than the best result obtained with the global implementation ($MSE = 37.47$ in Table V). The corresponding level-dependent implementations lead to similar values. Perhaps a more sophisticated threshold calculation method, instead of this ad-hoc procedure, would result in improvements.

B. Comparison of the Wavelet-based Denoising Methods

Table IX displays the results of all the denoising combinations explained, using the parameters described in Section III-A, for the Lena image. Fig. 4 and Fig. 5 display a few examples for $\sigma = 10$ and for $\sigma = 20$, respectively. The three main columns of Table IX report the MSE and SNR values corresponding to the three different noise levels, $\sigma = 10, 20,$ and 30. The first row indicates the MSE and SNR values for the noisy images, as a comparison for judging the denoised results. The remaining rows indicate the type of thresholding function and the thresholding rule that is used. The thresholding rules are prefixed with either S_- or P_-, depending on whether the thresholds were calculated globally (i.e. a Single threshold), or dependent on the level or subband (i.e. a Pyramid of thresholds). We implemented all the methods included in this study both level- or subband-dependently. However, because of the large number of the possible combinations, we only report the best of the two

approaches for each method. The boldfaced entry reflects the winning method with the smallest MSE and largest SNR, in this case the subband-dependent $SURE$ thresholding with the soft function, P_SURE, regardless of the noise level. We refer to this method as *SureShrink*. Similarly, the term *BayesShrink* denotes the subband-dependent P_Bayes implementation with the soft shrinkage function.

The corresponding results for the Goldhill and Einstein images are displayed in Table X and Table XI, respectively. Except for the different quantities involved, the main conclusions reached for the Lena image are valid for these two images as well. A minor difference appears in the case of Goldhill with $\sigma = 10$, where the *BayesShrink* method was the best, with $MSE = 42.44$. However, the second best method was *SureShrink*, with the very comparable $MSE = 42.57$. In all the other cases, just as for Lena, the winner was *SureShrink*, the runner-up was *BayesShrink*, and the other techniques lagged far behind in terms of MSE performance.

Next, we summarize the findings for the three test images, illustrating our observations with the results obtained for Lena.

• **Influence of Shrinkage Function**. As the values in Table IX indicate, in most cases, soft thresholding lead to estimates that were superior to the corresponding estimates obtained with the garrote shrinkage function, which, in turn, were superior to corresponding estimates obtained with the hard shrinkage function. For example, for the global *hypTest* method with $\sigma = 10$, the MSE values for the soft, garrote, and hard functions were 33.50, 36.12, and 72.39, respectively. This is expected as each pixel of the original image is contaminated by noise and a shrink or kill procedure would perform better than a keep or kill approach. An important exception occurred with the *universal* rule, when both hard and garrote thresholding resulted in better estimates than the corresponding ones using soft thresholding, regardless of the noise level. The optimal *SureShrink* method, however, led to much better denoising than did the best *universal* rule with hard thresholding (compare $MSE = 29.23$ to $MSE = 49.55$, for $\sigma = 10$). Subband-dependent semisoft thresholding results with the *top* rule were always inferior to the corresponding soft thresholding results. The global semisoft implementation, however, led to values comparable to the corresponding values obtained with soft thresholding in the $\sigma = 10$ and $\sigma = 20$ cases. Again, in our experiments, the optimal *SureShrink* method led to lower MSE values than the best method using the semisoft thresholding function.

We conclude that the choice of the shrinkage function strongly influences the results, and that soft thresholding is preferred to either garrote, hard or semisoft thresholding.

• **Influence of Shrinkage Rule**. Since soft thresholding resulted in the best estimates overall, we analyze the different rules by concentrating on the soft thresholding function. The conclusions are similar for the other thresholding functions.

The pyramidal implementations of the rules resulted in better estimates than their global counterparts regardless of the noise level, except for the case of the *minFDR* and the *hypTest* rules. For the *minFDR* method, the two implementations (pyramidal and global) lead to very similar results. For the *hypTest* method, the results depended on the amount of noise in the data: the pyramidal *hypTest* rule outperformed its global form when $\sigma = 10$, but underperformed when $\sigma = 20$ and $\sigma = 30$.

Despite the global implementation proposed in the literature [14], we found that subband-dependent *universal* thresholding outperformed its global version, regardless of the shrinkage function and the amount of noise in the image. For example, in the $\sigma = 10$ hard thresholding case, the global method re-

sulted in $MSE = 55.98$, while the subband-dependent one in $MSE = 49.55$.

The difference between the best two MSEs and the rest of the MSE values increased as σ increased. For example, at $\sigma = 10$, there were quite a few rules that resulted in comparable MSE values (P_SURE=29.23, P_Top=29.92, P_Bayes=30.26, P_HypTest=31.83), but at $\sigma = 30$ there was a larger gap (P_SURE=91.34, P_Bayes=92.74, S_SURE=113.01, S_Bayes=115.18). In the $\sigma = 10$ case, the second best method, after *SureShrink*, was the pyramidal *top*. The third was *BayesShrink*, with MSE close to the first two MSE values. At higher noise levels, the results of *BayesShrink* were close to the results of the still best *SureShrink*, but results with the *top* rule lagged behind. Since we want our results to be general, we exclude the *top* rule from the list of best denoisers.

Judging from the range of values in Table IX, the choice of the shrinkage rule strongly affects the outcome of the denoising operation. We found that the $SURE$ and the $Bayes$ rules were the best for our tests.

• **Influence of Noise**. Regardless of the noise level, the *SureShrink* method outperformed the other denoising methods that we considered. For $\sigma = 10$, the corresponding optimal MSE value was $MSE = 29.23$. Level-dependent *top* thresholding with soft shrinkage achieved an $MSE = 29.92$, very close to the optimal value, and *BayesShrink* came in third, with a still close $MSE = 30.26$. For $\sigma = 20$ and $\sigma = 30$, we have $MSE = 61.59$ and $MSE = 91.34$, respectively, for *SureShrink*. In both cases, *BayesShrink* was the second best denoiser, with the comparable values of $MSE = 63.33$ and $MSE = 92.74$, respectively.

Our main conclusion, stating that *SureShrink* and *BayesShrink* were the best denoisers overall, is not sensitive to the amount of noise in the images. The near-optimality of the level-dependent *top* rule with soft thresholding in the $\sigma = 10$ case was not consistent across the other noise levels and images, so we exclude it from the list of "good" denoisers. We think that choosing the optimal parameter for the *top* method needs more data-adaptive tuning than we proposed in Section III-A.

We stress that it is important to use a robust estimator of the noise. As explained in the second paragraph of Section III-A, our results were obtained using the global estimate $\hat{\sigma}$ based on the MAD of the coefficients from the HH_1 subband.

• **Influence of Wavelets**. Our findings are also robust across the wavelet used. The results in Table IX were obtained using the symmlet12 wavelet with 12 coefficients [1] with $K = 3$ multiresolution levels and periodic boundary treatment. We performed the same analyses using different wavelets, different numbers of levels, and different boundary extensions. In agreement with [9], we found that the choice of wavelet, the number of levels, and the boundary treatment rule had little effect on the results. The ordering of the methods, as measured by their MSE values, remained the same for the alternatives we tried. As an example, Table VII displays the MSE and SNR values of the winning *SureShrink* method for several wavelets and multiresolution levels. The values correspond to the $\sigma = 10$ case, and periodic boundary treatment. Tables XV through XX present some additional results, illustrating the effects of using different wavelets and different multiresoluion levels on different images.

In our study, the biorthogonal wavelets fared worse, as measured by the MSE, than the orthogonal symmlets. Because their symmetry leads to fewer visual artifacts in the reconstructed images, the biorthogonal wavelets are sometimes preferred over the orthogonal wavelets [6]. However, in our experi-

TABLE VII

Examples of MSE and SNR values for different wavelets and number of multiresolution levels.

Wavelet	K	MSE	SNR
Symmlet8	4	32.42	18.49
Symmlet8	3	31.14	18.67
Symmlet12	3	29.23	18.94
B-spline1.3	3	33.16	18.39
B-spline3.7	3	38.24	17.77

TABLE VIII

Estimate of the variance of the noise in the test images.

	$\sigma = 10$	$\sigma = 20$	$\sigma = 30$
Lena	120.01	386.47	828.44
Goldhill	148.07	412.25	858.92
Einstein	127.49	392.16	839.22

ments, the denoised images obtained with the nearly-symmetric orthogonal symmlets are visually comparable to the corresponding denoised images obtained with the biorthogonal wavelets.

• **VisuShrink Compared to SureShrink**. The authors in [14] define the term *VisuShrink* to refer to global soft thresholding with the *universal* threshold for one-dimensional signals, because it leads to visually pleasing results. However, for two-dimensional images, just as the authors in [6], we found that *SureShrink* yielded much better results, both in terms of MSE and visual quality, than the corresponding *VisuShrink* procedure. In fact, we found that even the global hard thresholding with the *universal* threshold ($MSE = 103.95$) outperformed VisuShrink ($MSE = 136.52$). To illustrate some of the typical artifacts resulting from non-optimal thresholding, Fig. 5 displays the original Lena image, its noisy $\sigma = 20$ counterpart, the best denoiser SureShrink ($MSE = 61.59$), and the result of applying the global *universal* threshold with the hard shrinkage function ($MSE = 103.95$). Notice the ringing around the edges and the blurring in the hair in the latter image. The same effect is also visible, although less pronounced, in Fig. 4 (d).

• **Final remarks**. Clearly, there is a wide range of variation in the quality of the denoised images. For example, for the $\sigma = 20$ image, although all methods decrease the $MSE = 399.50$ of the noisy image, the denoised MSE values range from the worst of 339.18 to the best of 61.59. Choosing the right method therefore has a large effect on the results.

In conclusion, we found that in our experiments *SureShrink* and *BayesShrink* were the best denoisers among the ones we studied. They yielded similar results and consistently outperformed the other methods in all but one case. *SureShrink* had slightly smaller MSE values than *BayesShrink* in most of the cases, but the differences were small enough to be just random fluctuations, and are in agreement with [9]. The denoised images using these two methods were generally indistinguishable to the human eye. Consequently, we do not recommend one method over the other, and rate them both number one, with a tie. However, because of the simplicity of the *BayesShrink* formula, some users might prefer it over *SureShrink*. One welcome property of these two winners is that they do not depend on any user-defined parameters, but are completely adaptive to the dataset at hand. We note that in the case of the Lena image with $\sigma = 10$, the level-dependent *top* method with soft shrinkage resulted in a slightly smaller MSE than *BayesShrink*. However, this one case seemed to be an anomaly and the result did not repeat consistently across the other noise levels and images. It is certainly possible to experiment further with the user-defined parameters of the various methods on a case-by-case basis and slightly reduce the MSE values for those methods. But, in general, *SureShrink* and *BayesShrink* achieved nearly optimal performance without any tuning of parameters.

IV. Comparison with Spatial Filters

While wavelet-based denoising techniques are certainly a powerful tool for image restoration, our study would be incomplete without a comparison with the more traditional approaches based on the use of spatial filters [32], [28]. In this section, we compare the effectiveness of denoising using several linear and non-linear filters applied either by themselves or in combination with other spatial filters. Our choice of filters is listed below, where the filter size is indicated in parenthesis:
• Mean filters ($3 \times 3, 5 \times 5$)
• Gaussian filters ($3 \times 3, 5 \times 5$)
• Scaled unsharp masking filters ($3 \times 3, 5 \times 5$). Given the real number β, these filters calculate

$$(1.0 + \beta)original\_image - (\beta)mean\_filtered\_image \quad (42)$$

In our experiments, $\beta = -0.8$ gave relatively good results.
• Alpha-trimmed mean filters ($3 \times 3, 5 \times 5$) with a trim size of either 1 or 2. The trim size is the number of smallest and largest pixels that are excluded in the calculation of the mean.
• Median filters ($3 \times 3, 5 \times 5$)
• Mid-point filters ($3 \times 3, 5 \times 5$). The value calculated is the average of the minimum and maximum within the filter mask.
• Minimum mean squared error filters ($3 \times 3, 5 \times 5$)
• Scaled unsharp masking filter (3×3) followed by a mean filter (3×3)
• Mean filter (3×3) applied twice
• Minimum mean squared error filter (5×5) followed by a mean filter (3×3)
• Minimum mean squared error filter (5×5) followed by a Gaussian filter (3×3)
• Scaled unsharp masking filter (3×3) followed by a Gaussian filter (3×3)
• Gaussian filter (3×3) applied twice

The minimum mean squared error filter requires the noise variance, which is usually unknown for many images. In order to obtain an estimate of the noise variance of an image with additive Gaussian noise, we use the following approach:
Step 1. Obtain a mean-filtered version of the image using a (3×3) filter.
Step 2. Subtract the mean filtered image from the original. This gives us a high pass version of the original image consisting of the noise and the edges.
Step 3. Obtain the standard deviation σ of the high pass image and drop all pixel values that are above σ or below $-\sigma$, thus removing the edge pixels.
Step 4. The standard deviation (or the MAD) of the remaining pixels gives an estimate of the standard deviation of the noise in the image.

For our test images, the values of the variance of the noise obtained using this method are given in Table VIII. These results indicate that the estimates obtained are reasonably close to the known values of the variance.

The MSE and SNR values for the Lena, Goldhill, and Einstein images as a result of denoising using spatial filters are given in Tables XII, XIII, and XIV. All our experiments use

periodic boundary treatment to handle values near the edges of the image. Examples of denoised versions of the Lena image with $\sigma = 20$ are given in Fig. 6.

The authors in [9] show empirically that the results of the best possible linear filtering, using the Wiener filter, are inferior to the results obtained with *SureShrink*. Comparing the *MSE* values in Tables XII, XIII, and XIV, to the corresponding values in Tables IX, X, and XI, however, indicates that combinations of spatial filters can be very competitive with wavelet-based denoising techniques.

The best spatial filter denoiser for the Lena image was the 5×5 minimum *MSE* filter followed by a 3×3 mean filter. Its *MSE* value was slightly higher than that of the best wavelet denoiser (compare 31.78 to 29.23) when $\sigma = 10$, but it achieved superior results when $\sigma = 20$ (compare 56.80 to 61.59) and when $\sigma = 30$ (compare 88.52 to 91.34). As Tables XIII and XIV indicate, there was no unique best denoiser for the Goldhill and Einstein images. Depending on the image and on the noise level, the optimal denoiser can be based either on a simple Gaussian filter, on a combination of a minimum *MSE* filter followed by a mean filter, or, on a combination of minimum *MSE* filter followed by a Gaussian filter.

Spatial filters are very simple to implement and are computationally faster than wavelet-based methods as they require far less computation in many cases. However, a comparison of the images indicates that the images that result from the application of spatial filters are often grainier than the ones obtained from wavelet techniques. This can be noticed in areas of the image that are relatively smooth, and around the edges which are better preserved in the wavelet denoised images. On the other hand, wavelet-based approaches sometime create noticeable artifacts that can substantially degrade the image.

V. Summary

In this paper, we evaluated several denoising methods on test images with known noise characteristics. We considered an extensive set of techniques based on statistical thresholding of wavelet coefficients as well as the more traditional approaches using spatial filters.

Based on our experiments, we conclude that *SureShrink* and *BayesShrink* are the best wavelet-based denoising methods for the types of images we considered, among the methods we considered. None of the other wavelet-based procedures that we examined achieved lower error rates, in terms of *MSE*, than these two techniques.

Comparing our results to relevant advances in denoising of images using wavelets, we find some agreements and some disagreements. For statistical reasons, such as near-optimality properties over a range of Besov spaces and continuity of the thresholding function, soft thresholding is the a-priori preferred choice of the authors in [9]. They only consider soft thresholding, and show that their newly proposed *BayesShrink* procedure outperforms *SureShrink* in most situations that they considered. Our analyses indicate empirically the superiority of the soft thresholding function in the test cases we investigated. In contrast, the authors in [24] use hard thresholding with the global *universal* rule to represent wavelet thresholding approaches in their work on comparing the denoising performance of wavelets and curvelets. Our study shows that *SureShrink* and *BayesShrink* achieve significantly better denoising results than the hard shrinkage using *universal* thresholds (Tables IX, X, and XI, and Fig. 5), suggesting that perhaps the former should be used in any comparison studies with competing procedures.

For completeness, we also compared the wavelet-based de-noisers with various spatial filter-based methods. Our results indicate that on an case-by-case basis, it is often possible to find a denoiser based on combinations of spatial filters that is superior to the best wavelet-based denoiser. In most, but not all, of those cases, that optimal method is given by the 5×5 Min-*MSE* filter followed by the 3×3 Gaussian filter. However, overall, there is no unique optimal denoiser of the former type for all the images and noise levels that we considered.

In addition to the denoising methods we considered in this study, there are several other alternatives. These include the use of non-decimated transforms [16], [23], [1] in the multiresolution decomposition, as well as the use of other basis functions, such as ridgelets and curvelets [4], [5]. The emerging research on curvelets indicates that, in certain cases, they offer improvements over the wavelets [24]. Different alternatives, such as partial differential equations-based techniques using level set [17] and total variation methods [8], and computational fluid dynamics approaches using essentially non-oscillatory (ENO) schemes [7] have also been proposed for image denoising. Hybrid denoisers, first selecting the best candidates of the different methods, then combining their results, might offer additional improvement in denoising performance.

References

[1] A. Bruce and H. Gao. *S+WAVELETS User's Manual*. StatSci Division of MathSoft, Inc., 1994.

[2] A. Bruce and H. Gao. *Applied Wavelet Analysis with S-PLUS*. Springer Verlag, 1996.

[3] C. Cai and P. de B. Harrington. Different discrete wavelet transforms applied to denoising analytical data. *J. Chem. Inf. Comput. Sci.*, 38:1161–1170, 1998.

[4] E.J. Candès. *Ridgelets: Theory and Applications*. PhD thesis, Stanford University, 1998.

[5] E.J. Candès and D.J. Donoho. Curvelets, multiresolution representation, and scaling laws. In A. Aldroubi, A. F. Laine, and M. A. Unser, editors, *Wavelet Applications in Signal and Image Processing VIII*, volume 4119. SPIE, 2000.

[6] A. Chambolle, R.A. DeVore, N. Lee, and B.J. Lucier. Nonlinear wavelet image processing: variational problems, compression, and noise removal through wavelets. *IEEE Trans. Image Processing*, 7:319–335, 1998.

[7] T. Chan and H Zhou. Adaptive ENO-wavelet transforms for discontinuous functions. Technical Report CAM 99-21, UCLA, 1999.

[8] T. Chan and H Zhou. Optimal construction of wavelet coefficients using total variation regularization in image compression. Technical Report CAM 00-27, UCLA, 2000.

[9] S.G. Chang, B. Yu, and M. Vetterli. Adaptive wavelet thresholding for image denoising and compression. *IEEE Trans. Image Processing*, 9:1532–1546, 2000.

[10] S.G. Chang, B. Yu, and M. Vetterli. Spatially adaptive wavelet thresholding based on context modeling for image denoising. *IEEE Trans. Image Processing*, 9:1522–1531, 2000.

[11] R.R. Coifman and D.L. Donoho. Translation-invariant de-noising. In A. Antoniadis and G. Oppenheim, editors, *Wavelets and Statistics*, Lecture Notes in Statistics, pages 125–150. Springer-Verlag, 1995.

[12] I. Daubechies. *Ten Lectures on Wavelets*. SIAM, 1992.

[13] R.A. DeVore and B.J. Lucier. Fast wavelet techniques for near-optimal processing. pages 48.3.1–48.3.7. IEEE Military Communications Conference, New York, 1992.

[14] D.L. Donoho and I. M. Johnstone. Ideal spatial adaptation via wavelet shrinkage. *Biometrika*, 81:425–455, 1994.

[15] D.L. Donoho and I. M. Johnstone. Adapting to unknown smoothness via wavelet shrinkage. *Journal of the American Statistical Association*, 90(432):1200–1224, December 1995.

[16] A. Dutilleux. An implementation of the 'algorithme á trous' to compute a wavelet transform. In J.M. Combes, A. Grossman, and Ph. Tchamitchian, editors, *Wavelets: Time-frequency Methods and Phase Space*, pages 298–304. Springer Verlag, 1987.

[17] R. Malladi and J. Sethian. A unified approach to noise removal, image enhancement, and shape recovery. *IEEE Trans. Image Processing*, 5, 1996.

[18] S.G. Mallat. A theory for multiresolution signal decomposition: The wavelet representation. *IEEE Trans. Pattern Analysis and Machine Intelligence*, 11:674–693, 1989.

[19] G.P. Nason and B.W. Silverman. The stationary wavelet transform and some statistical applications. In A. Antoniadis and G. Oppenheim, editors, *Wavelets and Statistics*, Lecture Notes in Statistics, pages 261–280. Springer-Verlag, 1995.

[20] R.T. Ogden. *Essential Wavelets for Statistical Applications and Data Analysis*. Birkhäuser, 1997.

[21] MR/1 Web Page. The MR/1 and MR/2 multiresolution software environment for image, signal and data processing. http://www.multiresolution.com/multires.htm.

[22] Sapphire Web Page. Sapphire: Large-scale data mining and pattern recognition. http://www.llnl.gov/casc/sapphire/.

[23] M.J. Shensa. The discrete wavelet transform: Wedding the á trous and Mallat algorithms. *IEEE Trans. Signal Processing*, 40:2464–2482, 1992.

[24] J.-L. Starck, E.J. Candès, and D.J. Donoho. The curvelet transform for image denoising. Department of Statistics, Stanford University, 2000.

[25] J.-L. Starck, F. Murtagh, and A. Bijaoui. *Image Processing and Data Analysis. The Multiscale Approach*. Cambridge University Press, 1998.

[26] C. Stein. Estimation of the mean of a multivariate normal distribution. *Annals of Statistics*, 9(6):1135–1151, 1981.

[27] A. Uhl. *Wavelets: adaptive and parallel methods in image coding and signal processing*. PhD thesis, University of Salzburg, 1996.

[28] S. Umbaugh. *Computer Vision and Image Processing: A Practical Approach using CVIPtools*. Prentice Hall, 1998.

[29] M. Unser. A practical guide to the implementation of the wavelet transform. In A. Aldroubi and M. Unser, editors, *Wavelets in Medicine and Biology*, pages 37–73. CRC Press, 1996.

[30] B. Vidakovic. *Statistical Modeling by Wavelets*. Wiley Series in Probability and Statistics. John Wiley & Sons, Inc., 1999.

[31] J.B. Weaver, X. Yansun, Jr. D.M. Healy, and L.D. Cromwell. Filtering noise from images with wavelet transforms. *Magnetic Resonance in Medicine*, 24:288–195, 1991.

[32] A. Weeks. *Fundamentals of Electronic Image Processing*. SPIE/IEEE Series on Imaging Science and Engineering. SPIE Optical Engineering Press and IEEE Press, 1996.
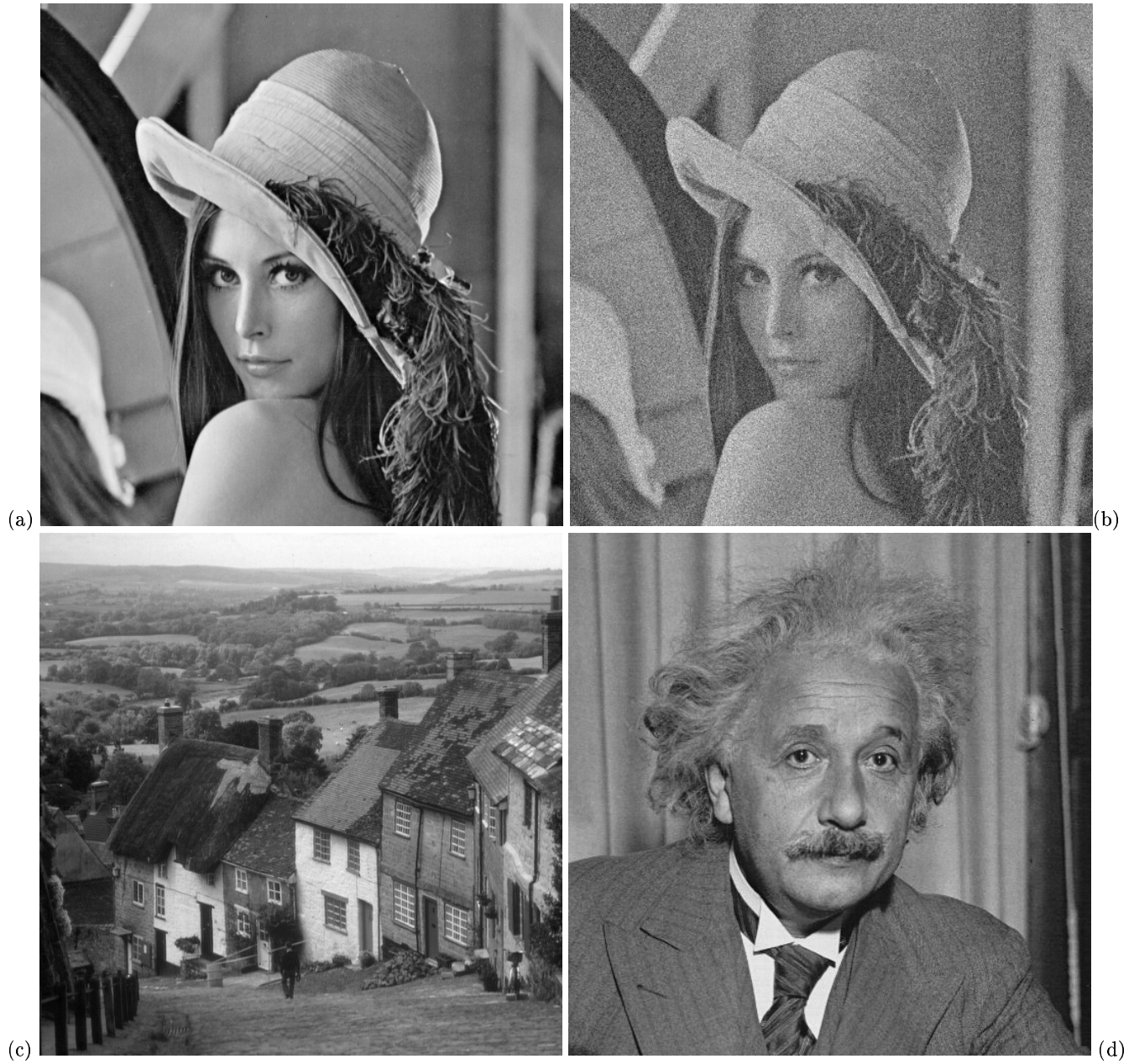
Fig. 3. Example test images. (a) Lena. (b) Lena corrupted with $\sigma = 30$ noise. (c) Goldhill. (d) Einstein.

Fig. 4. Denoising results with the Lena image with $\sigma = 10$, symmlet12 wavelet, three multiresolution levels, periodic boundary treatment. (a) *SureShrink*, $MSE = 29.23$. (b) Level-dependent *top* rule with soft thresholding, $MSE = 29.92$. (c) *BayesShrink*, $MSE = 30.26$. (d) Global *universal* rule with hard thresholding, $MSE = 55.98$.

Fig. 5. Wavelet-based results for the Lena image with $\sigma = 20$, symmlet12 wavelet, three multiresolution levels, periodic boundary treatment. (a) Original image. (b) Noisy image, $MSE = 399.50$. (c) *SureShrink*, $MSE = 61.59$. (d) Global *universal* rule with hard thresholding, $MSE = 103.95$.

(a)

(b)

Fig. 6. Filter-based results for the Lena image with $\sigma = 20$, spatial filters, periodic boundary treatment. (a) Minimum mean squared error (5×5) followed by Gaussian (3×3) filter, $MSE = 56.80$. (b) Minimum mean squared error (5×5) followed by mean (3×3) filter, $MSE = 64.80$.

TABLE IX

Wavelet-based results for the Lena image, the symmlet12 wavelet, three multiresolution levels and periodic boundary treatment.

	Rule	$\sigma = 10$		$\sigma = 20$		$\sigma = 30$	
		MSE	**SNR**	**MSE**	**SNR**	**MSE**	**SNR**
Noisy image		99.53	13.62	399.50	7.58	894.66	4.08
Soft	S_Universal	86.57	14.22	136.52	12.25	169.40	11.31
	S_MinFDR	33.26	18.38	81.13	14.51	143.89	12.02
	S_Top	33.35	18.37	91.46	13.99	177.24	11.11
	S_HypTest	33.50	18.35	103.12	13.47	261.45	9.42
	S_SURE	33.70	18.32	74.91	14.85	113.01	13.07
	S_Bayes	39.09	17.68	75.77	14.80	115.18	12.98
	P_Universal	76.45	14.76	123.54	12.68	156.90	11.64
	P_MinFDR	33.59	18.34	81.80	14.47	143.74	12.02
	P_Top	29.92	18.84	75.06	14.84	141.46	12.09
	P_HypTest	31.83	18.57	112.41	13.09	292.43	8.94
	P_SURE	**29.23**	**18.94**	**61.59**	**15.70**	**91.34**	**13.99**
	P_Bayes	30.26	18.79	63.33	15.58	92.74	13.93
Hard	S_Universal	55.98	16.12	103.95	13.43	142.44	12.06
	S_MinFDR	75.40	14.83	282.55	9.09	622.14	5.66
	S_Top	80.20	14.56	317.27	8.58	709.56	5.09
	S_HypTest	72.39	15.00	339.18	9.29	810.56	4.51
	S_SURE	70.23	15.13	257.76	9.49	562.66	6.10
	S_Bayes	92.38	13.94	240.58	9.79	255.64	9.52
	P_Universal	49.55	16.65	93.58	13.89	128.61	12.51
	P_MinFDR	75.11	14.84	280.66	9.12	618.50	5.69
	P_Top	68.56	15.24	263.28	9.39	584.97	5.93
	P_HypTest	76.71	14.75	351.63	8.14	829.56	4.41
	P_SURE	70.24	15.13	257.81	9.49	561.53	6.10
	P_Bayes	48.26	16.76	101.29	13.54	152.54	11.76
Garrote	S_Universal	69.81	15.16	121.28	12.76	158.12	11.61
	S_MinFDR	37.70	17.83	115.52	12.97	234.12	9.90
	S_Top	41.09	17.46	143.96	12.02	311.00	8.67
	S_HypTest	36.12	18.02	169.95	11.30	463.92	6.93
	S_Bayes	58.01	15.96	93.61	13.89	112.14	13.10
	P_Universal	60.98	15.75	107.77	13.27	143.52	12.03
	P_MinFDR	37.60	17.85	114.75	13.00	231.91	9.95
	P_Top	34.79	18.18	111.59	13.12	234.01	9.91
	P_HypTest	38.36	17.76	190.23	10.81	511.85	6.51
	P_Bayes	34.37	18.24	71.35	15.06	103.66	13.44
SemiSoft	S_Top	33.09	18.40	91.46	13.99	200.92	10.57
	P_Top	56.95	16.04	214.62	10.28	475.91	6.82

TABLE X

Wavelet-based results for the Goldhill image, the symmlet12 wavelet, three multiresolution levels and periodic boundary treatment.

		$\sigma = 10$		$\sigma = 20$		$\sigma = 30$	
	Rule	MSE	SNR	MSE	SNR	MSE	SNR
Noisy image		100.28	13.84	398.09	7.85	901.14	4.30
Soft	S_Universal	130.90	12.68	183.76	11.20	214.37	10.53
	S_MinFDR	49.39	16.91	105.90	13.60	174.68	11.42
	S_Top	48.78	16.96	111.08	13.39	199.68	10.84
	S_HypTest	50.25	16.83	122.25	12.97	283.68	9.32
	S_SURE	48.44	16.99	105.05	13.71	152.22	12.02
	S_Bayes	48.73	16.97	104.10	13.67	154.24	11.96
	P_Universal	118.58	13.10	170.79	11.52	204.18	10.75
	P_MinFDR	50.43	16.82	106.06	13.59	175.27	11.41
	P_Top	47.12	17.11	95.02	14.07	165.08	11.67
	P_HypTest	46.21	17.20	128.90	12.74	312.67	8.89
	P_SURE	42.57	17.55	**88.11**	**14.40**	**127.77**	**12.78**
	P_Bayes	**42.44**	**17.57**	90.07	14.30	128.22	12.77
Hard	S_Universal	92.83	14.17	152.47	12.01	194.45	10.96
	S_MinFDR	82.78	14.67	296.89	9.12	646.46	5.74
	S_Top	83.93	14.61	321.42	8.77	719.45	5.27
	S_HypTest	81.39	14.74	345.97	8.45	823.85	4.69
	S_SURE	79.29	14.85	274.51	9.46	589.84	6.14
	S_Bayes	95.43	14.05	272.17	9.50	347.42	8.44
	P_Universal	83.70	14.62	139.17	12.41	180.27	11.29
	P_MinFDR	82.97	14.66	295.40	9.14	644.87	5.75
	P_Top	73.94	15.16	269.67	9.54	597.29	6.08
	P_HypTest	83.86	14.61	356.30	8.33	841.29	5.60
	P_SURE	79.30	14.85	274.41	9.46	589.37	6.14
	P_Bayes	68.48	15.49	137.88	12.45	205.15	10.72
Garrote	S_Universal	111.67	13.37	169.87	11.54	207.24	10.68
	S_MinFDR	49.84	16.87	136.87	12.48	262.87	9.65
	S_Top	50.34	16.83	156.45	11.90	325.61	8.72
	S_HypTest	49.36	16.91	185.74	11.16	484.63	6.99
	S_Bayes	65.33	15.69	123.64	12.92	157.47	11.87
	P_Universal	99.95	13.85	155.36	11.93	194.23	10.96
	P_MinFDR	50.26	16.83	136.07	12.51	261.91	9.66
	P_Top	46.20	17.20	125.79	12.85	252.93	9.82
	P_HypTest	49.70	16.88	203.35	10.76	530.43	6.60
	P_Bayes	46.91	17.13	98.27	13.92	142.73	12.30
SemiSoft	S_Top	57.19	16.27	116.67	13.18	230.12	10.23
	P_Top	67.48	15.55	226.15	10.30	491.77	6.93

TABLE XI

WAVELET-BASED RESULTS FOR THE EINSTEIN IMAGE, THE SYMMLET12 WAVELET, THREE MULTIRESOLUTION LEVELS AND PERIODIC BOUNDARY TREATMENT.

		$\sigma = 10$		$\sigma = 20$		$\sigma = 30$	
	Rule	**MSE**	**SNR**	**MSE**	**SNR**	**MSE**	**SNR**
Noisy image		100.28	10.10	398.09	4.11	901.14	0.56
Soft	S_Universal	87.14	10.71	117.77	9.40	139.02	8.68
	S_MinFDR	40.87	14.00	85.56	10.79	145.87	8.47
	S_Top	40.52	14.03	95.25	10.32	179.14	7.58
	S_HypTest	41.36	13.94	107.00	9.81	266.06	5.86
	S_SURE	41.09	13.97	78.80	11.14	110.28	9.68
	S_Bayes	41.90	13.89	78.81	11.14	112.88	9.58
	P_Universal	80.45	11.05	110.54	9.67	132.42	8.89
	P_MinFDR	41.87	13.89	86.15	10.76	145.16	8.49
	P_Top	38.11	14.30	80.82	11.03	148.17	8.40
	P_HypTest	39.12	14.18	116.18	9.46	297.96	5.37
	P_SURE	**36.80**	**14.45**	**68.65**	**11.74**	**95.44**	**10.31**
	P_Bayes	37.24	14.40	69.98	11.66	95.45	10.31
Hard	S_Universal	67.85	11.79	100.79	10.07	124.86	9.15
	S_MinFDR	81.41	11.00	288.32	5.51	631.20	2.11
	S_Top	83.67	10.88	320.13	5.05	717.94	1.55
	S_HypTest	79.23	11.12	341.63	4.77	819.73	0.97
	S_SURE	77.45	11.22	264.56	5.88	570.96	2.54
	S_Bayes	92.07	10.47	199.50	7.11	201.72	7.06
	P_Universal	62.75	12.13	93.53	10.40	118.49	9.37
	P_MinFDR	81.57	10.99	287.12	5.53	627.14	2.14
	P_Top	72.60	11.50	266.90	5.85	593.38	2.38
	P_HypTest	82.20	10.96	352.90	4.63	838.31	0.87
	P_SURE	77.46	11.22	264.67	5.88	573.55	2.52
	P_Bayes	63.15	12.10	105.87	9.86	157.80	8.13
Garrote	S_Universal	77.17	11.23	109.73	9.71	132.89	8.87
	S_MinFDR	45.37	13.54	122.18	9.24	239.80	6.31
	S_Top	46.84	13.40	148.64	8.39	315.09	5.12
	S_HypTest	44.30	13.64	174.80	7.68	471.79	3.37
	S_Bayes	56.81	12.56	85.39	10.79	109.77	9.70
	P_Universal	70.80	11.61	101.98	10.02	125.32	9.13
	P_MinFDR	45.77	13.50	121.47	9.26	237.14	6.36
	P_Top	41.52	13.93	117.49	9.41	242.20	6.27
	P_HypTest	45.65	13.51	194.34	7.22	520.16	2.95
	P_Bayes	41.73	13.90	76.85	11.25	104.69	9.91
SemiSoft	S_Top	44.94	13.58	107.29	9.80	221.41	6.66
	P_Top	63.89	12.05	221.54	6.65	485.92	3.24

TABLE XII

Spatial filter-based results for the Lena image with periodic boundary treatment.

Image	$\sigma = 10$		$\sigma = 20$		$\sigma = 30$	
	MSE	SNR	MSE	SNR	MSE	SNR
Noisy image	99.53	13.62	399.50	7.58	894.66	4.08
Mean (3)	42.67	17.30	76.34	14.77	130.46	12.44
Mean (5)	82.07	14.46	93.91	13.87	113.59	13.05
Gaussian (3)	32.95	18.42	95.25	13.81	196.92	10.66
Gaussian (5)	45.58	17.01	67.09	15.33	101.58	13.53
Scaled Unsharp Masking (3)	34.84	18.18	79.13	14.62	150.75	11.82
Scaled Unsharp Masking (5)	57.79	15.98	81.32	14.50	119.63	12.82
Alpha Trimmed Mean (3,1)	39.12	17.68	76.11	14.78	134.52	12.31
Alpha Trimmed Mean (5,2)	74.20	14.89	88.48	14.13	110.41	13.17
Median (3)	40.16	17.56	94.50	13.84	178.17	11.09
Median (5)	59.31	15.87	84.41	14.33	120.39	12.79
Mid-point (3)	78.76	14.64	131.29	12.42	222.31	10.13
Mid-point (5)	178.00	11.09	196.15	10.67	249.49	9.63
Min-MSE (3)	70.67	15.11	192.53	10.75	389.93	7.69
Min-MSE (5)	39.35	17.65	91.97	13.96	163.36	11.47
S-Unsharp (3), Mean (3)	50.50	16.57	69.00	15.21	98.65	13.66
Mean (3), Mean (3)	54.07	16.27	70.67	15.11	97.35	13.72
Min-MSE (5), Mean (3)	44.95	17.07	64.80	15.48	89.44	14.08
Min-MSE (5), Gaussian (3)	**31.78**	**18.58**	**56.80**	**16.06**	**88.52**	**14.13**
S-Unsharp (3), Gaussian (3)	41.56	17.41	66.99	15.34	107.81	13.27
Gaussian (3), Gaussian (3)	37.09	17.91	68.64	15.23	119.50	12.83

TABLE XIII

Spatial filter-based results for the Goldhill image with periodic boundary treatment.

Image	$\sigma = 10$		$\sigma = 20$		$\sigma = 30$	
	MSE	SNR	MSE	SNR	MSE	SNR
Noisy image	100.28	13.84	398.09	7.85	901.14	4.30
Mean (3)	70.66	15.35	103.61	13.69	159.69	11.81
Mean (5)	118.84	13.10	130.92	12.68	150.56	12.07
Gaussian (3)	**43.23**	**17.49**	104.99	13.63	209.47	10.63
Gaussian (5)	69.31	15.44	90.57	14.28	126.10	12.84
Scaled Unsharp Masking (3)	52.90	16.61	96.54	14.00	170.55	11.53
Scaled Unsharp Masking (5)	81.51	14.73	105.03	13.63	143.90	12.27
Alpha Trimmed Mean (3,1)	66.87	15.59	103.27	13.71	163.42	11.71
Alpha Trimmed Mean (5,2)	112.43	13.34	126.57	12.82	148.22	12.14
Median (3)	65.24	15.70	119.50	13.07	206.30	10.70
Median (5)	95.47	14.05	121.43	13.00	157.77	11.87
Mid-point (3)	107.57	13.53	159.92	11.81	254.28	9.79
Mid-point (5)	198.11	10.88	223.84	10.35	278.38	9.40
Min-MSE (3)	102.12	13.75	214.07	10.54	420.92	7.60
Min-MSE (5)	59.10	16.13	112.05	13.35	186.82	11.13
S-Unsharp (3), Mean (3)	76.76	14.99	95.05	14.07	125.53	12.86
Mean (3), Mean (3)	80.14	14.81	96.65	13.99	123.94	12.91
Min-MSE (5), Mean (3)	81.12	14.75	100.51	13.82	125.80	12.85
Min-MSE (5), Gaussian (3)	57.45	16.25	**84.51**	**14.58**	**119.08**	**13.09**
S-Unsharp (3), Gaussian (3)	64.08	15.78	89.15	14.34	131.31	12.66
Gaussian (3), Gaussian (3)	55.64	16.39	86.83	14.46	139.32	12.41

TABLE XIV

Spatial filter-based results for the Einstein image with periodic boundary treatment.

Image	$\sigma = 10$		$\sigma = 20$		$\sigma = 30$	
	MSE	SNR	MSE	SNR	MSE	SNR
Noisy image	100.28	10.10	398.09	4.11	901.14	0.56
Mean (3)	49.80	13.14	82.66	10.94	138.87	8.68
Mean (5)	76.29	11.28	87.65	10.68	107.64	9.79
Gaussian (3)	**36.14**	**14.53**	97.73	10.21	202.20	7.05
Gaussian (5)	48.00	13.30	68.82	11.73	104.61	9.91
Scaled Unsharp Masking (3)	39.50	14.14	83.00	10.92	157.05	8.15
Scaled Unsharp Masking (5)	54.20	12.77	77.10	11.24	116.21	9.46
Alpha Trimmed Mean (3,1)	47.72	13.32	83.47	10.89	143.51	8.54
Alpha Trimmed Mean (5,2)	71.73	11.55	84.63	10.83	106.26	9.85
Median (3)	49.78	13.14	102.43	10.01	188.06	7.37
Median (5)	61.68	12.21	84.34	10.85	119.37	9.34
Mid-point (3)	78.33	11.17	132.11	8.90	227.41	6.54
Mid-point (5)	139.32	8.67	168.03	7.86	226.30	6.56
Min-MSE (3)	78.08	11.18	196.54	7.17	404.35	4.04
Min-MSE (5)	46.60	13.43	93.85	10.39	163.17	7.98
S-Unsharp (3), Mean (3)	52.34	12.92	70.15	11.65	100.92	10.07
Mean (3), Mean (3)	54.38	12.76	70.33	11.64	97.95	10.20
Min-MSE (5), Mean (3)	55.04	12.70	70.49	11.63	**92.51**	**10.45**
Min-MSE (5), Gaussian (3)	43.34	13.74	**64.86**	**11.99**	94.25	10.37
S-Unsharp (3), Gaussian (3)	45.04	13.57	69.77	11.67	112.13	9.61
Gaussian (3), Gaussian (3)	40.76	14.01	71.63	11.56	124.29	9.17

TABLE XV

Wavelet-based results for the Lena image, the symmlet8 wavelet, four multiresolution levels and periodic boundary treatment.

		$\sigma = 10$		$\sigma = 20$		$\sigma = 30$	
	Method	**MSE**	**SNR**	**MSE**	**SNR**	**MSE**	**SNR**
Noisy image		99.53	13.62	399.50	7.58	894.66	4.08
Soft	S_Universal	103.92	13.43	178.33	11.09	237.39	9.84
	S_MinFDR	36.56	17.97	84.49	14.33	146.70	11.93
	S_Top	36.50	17.98	93.63	13.88	178.38	11.09
	S_HypTest	36.84	17.94	106.07	13.34	261.56	9.42
	S_SURE	36.56	17.97	80.50	14.54	124.16	12.66
	S_Adapt	36.56	17.97	80.50	14.54	124.16	12.66
	S_Bayes	53.00	16.36	100.79	13.56	127.73	12.54
	P_Universal	87.78	14.16	150.79	11.82	202.27	10.54
	P_MinFDR	38.64	17.73	89.16	14.10	148.80	11.87
	P_Top	33.14	18.39	77.68	14.70	144.78	11.99
	P_HypTest	34.70	18.20	114.80	13.00	292.36	8.95
	P_SURE	32.42	18.49	64.00	15.54	93.10	13.91
	P_Adapt	32.47	18.48	64.00	15.54	93.94	13.87
	P_Bayes	34.19	18.26	66.90	15.34	95.64	13.79
Hard	S_Universal	61.58	15.70	116.62	12.93	167.80	11.35
	S_MinFDR	80.55	14.54	285.39	9.04	618.71	5.68
	S_Top	84.84	14.31	320.69	8.54	710.89	5.08
	S_HypTest	77.86	14.69	345.52	8.21	816.34	4.48
	S_SURE	75.26	14.83	263.31	9.39	558.03	6.13
	S_Adapt	75.26	14.83	263.31	9.39	558.03	6.13
	S_Bayes	103.05	13.47	336.77	8.33	494.30	6.66
	P_Universal	53.81	16.29	101.09	13.55	143.16	12.04
	P_MinFDR	80.48	14.54	287.77	9.00	617.45	5.69
	P_Top	73.38	14.94	268.31	9.31	590.12	5.89
	P_HypTest	82.33	14.44	357.97	8.06	835.94	4.38
	P_SURE	75.27	14.83	263.21	9.40	557.96	6.13
	P_Adapt	62.93	15.61	152.21	11.77	159.77	11.56
	P_Bayes	54.86	16.21	105.69	13.35	152.93	11.75
Garrote	S_Universal	77.86	14.69	143.84	12.02	201.73	10.55
	S_MinFDR	41.12	17.46	116.32	12.94	231.03	9.96
	S_Top	44.05	17.16	144.41	12.00	308.84	8.70
	S_HypTest	39.67	17.61	173.59	11.20	464.174	6.93
	S_Bayes	78.68	14.64	161.93	11.51	166.27	11.39
	P_Universal	66.15	15.39	120.81	12.78	168.77	11.33
	P_MinFDR	41.34	17.45	118.83	12.85	230.59	9.97
	P_Top	38.61	17.73	114.89	13.00	239.76	9.80
	P_HypTest	42.26	17.34	194.56	10.71	513.67	6.49
	P_Bayes	39.13	17.67	76.45	14.76	108.78	13.23
SemiSoft	S_Top	37.46	17.86	84.09	14.35	181.31	11.01
	P_Top	61.12	15.74	217.46	10.22	477.55	6.81

TABLE XVI

Wavelet-based results for the Lena image, the symmlet8 wavelet, three multiresolution levels and periodic boundary treatment.

		$\sigma = 10$		$\sigma = 20$		$\sigma = 30$	
	Method	MSE	SNR	MSE	SNR	MSE	SNR
Noisy image		99.53	13.62	399.50	7.58	894.66	4.08
Soft	S_Universal	88.45	14.13	139.93	12.14	175.89	11.15
	S_MinFDR	34.58	18.21	81.62	14.48	143.40	12.03
	S_Top	34.74	18.19	92.16	13.95	178.36	11.09
	S_HypTest	34.74	18.19	104.47	13.41	261.63	9.42
	S_SURE	34.83	18.18	75.66	14.81	114.90	13.00
	S_Adapt	34.83	18.18	75.66	14.81	114.90	13.00
	S_Bayes	41.59	17.41	76.99	14.73	118.80	12.85
	P_Universal	78.11	14.67	126.48	12.58	162.50	11.49
	P_MinFDR	34.83	18.18	82.28	14.45	143.28	12.04
	P_Top	31.88	18.56	76.76	14.75	144.37	12.00
	P_HypTest	33.36	18.37	114.14	13.02	292.97	8.93
	P_SURE	31.14	18.67	63.32	15.58	93.61	13.89
	P_Adapt	31.19	18.66	63.32	15.58	94.46	13.85
	P_Bayes	32.84	18.43	66.04	15.40	95.93	13.78
Hard	S_Universal	57.32	16.01	105.49	13.37	147.27	11.92
	S_MinFDR	79.06	14.62	285.28	9.05	617.99	5.69
	S_Top	83.94	14.36	321.05	8.53	712.83	5.07
	S_HypTest	76.43	14.77	344.09	8.23	814.94	4.49
	S_SURE	73.78	14.92	262.39	9.41	557.93	6.13
	S_Adapt	73.78	14.92	262.39	9.41	557.93	6.13
	S_Bayes	97.22	13.72	252.55	9.57	235.09	9.89
	P_Universal	51.13	16.51	95.43	13.80	132.28	12.38
	P_MinFDR	78.87	14.63	285.88	9.04	615.71	5.70
	P_Top	71.95	15.03	266.91	9.33	588.64	5.90
	P_HypTest	80.88	14.52	356.59	8.07	834.44	4.38
	P_SURE	73.80	14.92	261.64	9.42	556.25	6.15
	P_Adapt	61.47	15.71	150.64	11.82	158.03	11.61
	P_Bayes	53.43	16.32	104.29	13.42	151.47	11.79
Garrote	S_Universal	71.15	15.08	123.24	12.69	163.95	11.45
	S_MinFDR	39.77	17.60	116.37	12.94	231.79	9.95
	S_Top	43.22	17.24	145.51	11.97	312.88	8.64
	S_HypTest	38.34	17.76	172.90	11.22	464.50	6.92
	S_Bayes	42.99	15.66	98.27	13.67	112.19	13.10
	P_Universal	62.23	15.66	109.68	13.20	148.26	11.89
	P_MinFDR	39.69	17.61	116.80	12.92	230.30	9.98
	P_Top	37.20	17.89	113.55	13.05	238.41	9.82
	P_HypTest	40.94	17.48	193.57	10.73	513.03	6.50
	P_Bayes	37.70	17.83	75.14	14.84	107.76	13.27
SemiSoft	S_Top	34.99	18.16	91.21	14.00	200.82	10.57
	P_Top	59.41	15.86	216.55	10.24	478.16	6.80

TABLE XVII

Wavelet-based results for the Goldhill image, the symmlet8 wavelet, four multiresolution levels and periodic boundary treatment.

		$\sigma = 10$		$\sigma = 20$		$\sigma = 30$	
	Method	**MSE**	**SNR**	**MSE**	**SNR**	**MSE**	**SNR**
Noisy image		100.28	13.83	398.09	7.85	901.14	4.30
Soft	S_Universal	147.30	12.16	223.04	10.36	274.05	9.47
	S_MinFDR	52.60	16.63	110.17	13.42	177.84	11.34
	S_Top	52.52	16.64	114.09	13.27	199.97	10.84
	S_HypTest	53.46	16.56	125.63	12.85	285.28	9.29
	S_SURE	50.70	16.79	109.21	13.46	160.47	11.79
	S_Adapt	50.70	16.79	109.21	13.46	160.47	11.79
	S_Bayes	59.64	16.09	121.89	12.99	166.13	11.64
	P_Universal	128.93	12.74	195.22	10.94	241.27	10.02
	P_MinFDR	54.70	16.46	111.34	13.38	182.09	11.42
	P_Top	50.42	16.82	98.34	13.92	166.15	11.64
	P_HypTest	49.05	16.94	131.86	12.64	314.06	8.88
	P_SURE	46.38	17.18	91.40	14.23	127.25	12.80
	P_Adapt	46.43	17.18	91.40	14.23	128.01	12.77
	P_Bayes	46.55	17.16	94.15	14.11	128.50	12.76
Hard	S_Universal	99.61	13.86	163.92	11.70	214.23	10.54
	S_MinFDR	89.08	14.35	303.24	9.03	651.72	5.70
	S_Top	89.24	14.34	325.66	8.72	721.80	5.26
	S_HypTest	87.61	14.42	353.10	8.37	831.92	4.64
	S_SURE	83.20	14.63	281.16	9.36	597.72	6.08
	S_Adapt	83.20	14.63	281.16	9.36	597.72	6.08
	S_Bayes	104.93	13.64	346.48	9.45	581.70	6.20
	P_Universal	88.04	14.40	144.92	12.23	188.78	11.09
	P_MinFDR	88.86	14.36	302.92	9.03	651.45	5.71
	P_Top	79.58	14.84	276.39	9.43	602.41	6.05
	P_HypTest	90.33	14.29	363.53	8.24	848.33	4.56
	P_SURE	85.49	14.53	281.24	9.35	597.40	6.08
	P_Adapt	73.78	15.17	226.19	10.30	316.87	8.84
	P_Bayes	75.88	15.04	144.45	12.25	208.62	10.65
Garrote	S_Universal	119.94	13.06	191.74	11.02	243.8	9.97
	S_MinFDR	53.76	16.54	140.55	12.37	264.02	9.63
	S_Top	53.84	16.53	157.83	11.86	323.20	8.75
	S_HypTest	53.17	16.59	190.12	11.05	488.78	6.95
	S_Bayes	83.19	14.64	180.94	11.27	222.96	10.36
	P_Universal	105.14	13.63	166.67	11.63	211.66	10.59
	P_MinFDR	53.98	16.52	140.54	12.37	265.16	9.61
	P_Top	50.47	16.81	130.59	12.69	255.62	9.77
	P_HypTest	54.10	16.51	208.55	10.65	535.62	6.55
	P_Bayes	52.76	16.63	103.96	13.68	144.99	12.23
SemiSoft	S_Top	63.19	15.84	114.07	13.27	213.76	10.55
	P_Top	72.92	15.22	231.67	10.20	494.84	6.90

TABLE XVIII

Wavelet-based results for the Goldhill image, the symmlet8 wavelet, three multiresolution levels and periodic boundary treatment.

		$\sigma = 10$		$\sigma = 20$		$\sigma = 30$	
	Method	MSE	SNR	MSE	SNR	MSE	SNR
Noisy image		100.28	13.83	398.09	7.85	901.14	4.30
Soft	S_Universal	129.70	12.72	181.64	11.25	211.64	10.59
	S_MinFDR	50.44	16.82	106.52	13.57	173.89	11.44
	S_Top	50.04	16.85	111.74	13.36	198.98	10.86
	S_HypTest	51.09	16.76	123.57	12.93	284.92	9.29
	S_SURE	48.96	16.95	104.56	13.65	150.48	12.07
	S_Adapt	48.96	16.95	104.56	13.65	150.48	12.07
	S_Bayes	51.35	16.74	104.63	13.65	151.424	12.04
	P_Universal	117.83	13.13	168.57	11.58	200.30	10.83
	P_MinFDR	50.91	16.78	106.88	13.56	174.53	11.43
	P_Top	49.08	16.94	97.32	13.96	165.69	11.65
	P_HypTest	47.59	17.07	130.94	12.67	314.46	8.87
	P_SURE	44.94	17.32	90.52	14.28	127.64	12.79
	P_Adapt	44.99	17.31	90.52	14.28	128.40	12.76
	P_Bayes	45.11	17.30	93.13	14.15	128.69	12.75
Hard	S_Universal	94.53	14.09	149.81	12.09	188.33	11.10
	S_MinFDR	87.34	14.43	301.29	9.06	651.03	5.71
	S_Top	88.21	14.39	325.86	8.71	723.60	5.25
	S_HypTest	86.03	14.50	351.46	8.39	830.43	4.65
	S_SURE	83.85	14.61	279.32	9.38	596.00	6.09
	S_Adapt	83.85	14.61	279.32	9.38	596.00	6.09
	S_Bayes	100.77	13.81	280.50	9.37	368.38	8.18
	P_Universal	84.82	14.56	137.08	12.48	175.42	11.40
	P_MinFDR	87.15	14.44	300.94	9.06	649.21	5.72
	P_Top	78.06	14.92	274.85	9.45	600.92	6.06
	P_HypTest	88.80	14.36	361.97	8.26	846.92	4.57
	P_SURE	83.89	14.61	279.24	9.39	595.36	6.09
	P_Adapt	72.18	15.26	224.20	10.34	314.83	8.86
	P_Bayes	74.36	15.13	142.91	12.29	207.20	10.68
Garrote	S_Universal	111.59	13.37	167.53	11.60	202.29	10.79
	S_MinFDR	52.18	16.67	139.04	12.41	263.96	9.63
	S_Top	52.59	16.64	158.31	11.85	326.55	8.71
	S_HypTest	51.66	16.71	188.93	11.08	488.59	6.96
	S_Bayes	70.22	15.38	127.12	12.80	158.40	11.85
	P_Universal	100.25	13.83	153.13	11.99	188.66	11.09
	P_MinFDR	52.20	16.67	138.88	12.41	263.02	9.64
	P_Top	48.98	16.94	129.12	12.74	254.25	9.79
	P_HypTest	52.65	16.63	207.30	10.68	534.80	6.56
	P_Bayes	51.25	16.75	102.52	13.74	144.00	12.26
SemiSoft	S_Top	58.54	16.17	118.52	13.11	231.63	10.20
	P_Top	70.02	15.39	229.87	10.23	494.38	6.90

TABLE XIX

Wavelet-based results for the Einstein image, the symmlet8 wavelet, four multiresolution levels and periodic boundary treatment.

		$\sigma = 10$		$\sigma = 20$		$\sigma = 30$	
	Method	**MSE**	**SNR**	**MSE**	**SNR**	**MSE**	**SNR**
Noisy image		100.28	10.10	398.09	4.11	901.14	0.56
Soft	S_Universal	100.31	10.10	147.30	8.43	181.90	7.51
	S_MinFDR	42.74	13.80	87.72	10.68	145.92	8.47
	S_Top	42.45	13.83	96.20	10.28	176.93	7.63
	S_HypTest	43.34	13.74	108.46	9.76	264.03	5.89
	S_SURE	42.32	13.84	82.45	10.95	116.18	9.46
	S_Adapt	42.32	13.84	82.45	10.95	116.18	9.46
	S_Bayes	50.27	13.10	90.53	10.54	116.79	9.43
	P_Universal	88.87	10.62	129.52	8.99	160.83	8.05
	P_MinFDR	45.06	13.57	88.07	10.66	146.51	8.45
	P_Top	39.64	14.13	82.00	10.97	147.77	8.41
	P_HypTest	40.45	14.04	117.25	9.42	296.07	5.39
	P_SURE	38.30	14.28	69.16	11.71	93.60	10.40
	P_Adapt	38.56	14.25	69.18	11.71	94.01	10.38
	P_Bayes	38.94	14.20	70.98	11.60	94.15	10.37
Hard	S_Universal	71.74	11.55	110.79	9.66	142.97	8.56
	S_MinFDR	84.33	10.85	292.30	5.45	634.00	2.09
	S_Top	85.78	10.78	321.56	5.04	717.79	1.55
	S_HypTest	82.18	10.96	344.88	4.73	823.34	0.95
	S_SURE	80.28	11.06	269.02	5.81	573.50	2.52
	S_Adapt	80.28	11.06	269.02	5.81	573.50	2.52
	S_Bayes	100.00	10.11	303.97	5.28	406.30	4.02
	P_Universal	65.37	11.96	98.92	10.16	126.95	9.07
	P_MinFDR	84.41	10.85	290.59	5.48	630.32	2.11
	P_Top	75.03	11.36	270.07	5.79	595.70	3.36
	P_HypTest	85.19	10.81	356.26	4.59	842.30	0.85
	P_SURE	80.27	11.06	268.52	5.82	573.46	2.52
	P_Adapt	68.32	11.76	212.98	6.82	167.58	7.87
	P_Bayes	66.52	11.88	112.52	9.60	156.29	8.17
Garrote	S_Universal	83.57	10.89	127.36	9.06	161.85	8.02
	S_MinFDR	47.11	13.38	123.55	9.19	238.41	6.34
	S_Top	48.01	13.30	148.45	8.38	311.43	5.18
	S_HypTest	45.99	13.48	176.76	7.63	471.39	3.38
	S_Bayes	72.89	11.48	132.64	8.88	137.73	8.72
	P_Universal	74.58	11.38	111.58	9.63	141.83	8.59
	P_MinFDR	47.68	13.33	122.52	9.23	236.24	6.38
	P_Top	43.28	13.75	119.52	9.33	243.89	6.24
	P_HypTest	47.433	13.35	196.95	7.17	521.11	2.94
	P_Bayes	44.11	13.66	79.76	11.09	105.08	9.89
SemiSoft	S_Top	47.27	13.36	100.39	10.09	203.10	7.03
	P_Top	66.21	11.90	222.70	6.63	485.43	3.25

TABLE XX

Wavelet-based results for the Einstein image, the symmlet8 wavelet, three multiresolution levels and periodic boundary treatment.

	Method	$\sigma = 10$		$\sigma = 20$		$\sigma = 30$	
		MSE	**SNR**	**MSE**	**SNR**	**MSE**	**SNR**
Noisy image		100.28	10.10	398.09	4.11	901.14	0.56
Soft	S_Universal	87.43	10.69	119.78	9.32	142.20	8.58
	S_MinFDR	41.38	13.94	86.10	10.76	145.16	8.49
	S_Top	41.08	13.97	95.76	10.30	179.11	7.58
	S_HypTest	41.82	13.89	107.91	9.78	266.07	5.86
	S_SURE	41.22	13.96	78.88	11.14	109.88	9.70
	S_Adapt	41.22	13.96	78.88	11.14	109.88	9.70
	S_Bayes	42.94	13.78	78.85	11.14	113.55	9.56
	P_Universal	80.63	11.04	111.75	9.63	135.26	8.80
	P_MinFDR	41.92	13.88	86.01	10.76	145.25	8.49
	P_Top	39.10	14.19	81.77	10.98	148.27	8.40
	P_HypTest	39.74	14.12	117.44	9.41	298.16	5.36
	P_SURE	37.78	14.34	69.39	11.69	95.85	10.29
	P_Adapt	38.03	14.31	69.41	11.69	96.26	10.27
	P_Bayes	38.38	14.27	71.01	11.60	96.03	10.28
Hard	S_Universal	67.77	11.80	101.25	10.05	128.79	9.01
	S_MinFDR	83.45	10.89	292.10	5.45	632.16	2.10
	S_Top	85.44	10.79	322.29	5.03	719.95	1.53
	S_HypTest	81.47	11.00	344.22	4.74	822.80	0.95
	S_SURE	79.56	11.10	267.89	5.83	572.95	2.52
	S_Adapt	79.56	11.10	267.89	5.83	572.95	2.52
	S_Bayes	94.71	10.34	214.14	6.80	196.69	7.17
	P_Universal	63.08	12.11	93.80	10.39	119.92	9.32
	P_MinFDR	83.44	10.89	289.74	5.49	629.922	2.11
	P_Top	74.38	11.39	269.42	5.80	595.17	2.36
	P_HypTest	84.53	10.84	355.59	4.60	841.72	0.86
	P_SURE	79.55	11.10	267.67	5.83	572.93	2.53
	P_Adapt	67.60	11.81	212.13	6.84	167.04	7.88
	P_Bayes	65.87	11.92	111.87	9.62	155.77	8.18
Garrote	S_Universal	76.96	11.25	111.06	9.65	136.41	8.76
	S_MinFDR	46.33	13.45	123.72	9.18	239.10	6.32
	S_Top	47.65	13.33	149.88	8.35	316.07	5.11
	S_HypTest	45.29	13.55	176.77	7.63	472.88	3.36
	S_Bayes	59.07	12.40	88.78	10.63	109.37	9.72
	P_Universal	70.74	11.61	102.46	10.00	128.15	9.03
	P_MinFDR	46.46	13.44	122.18	9.24	237.65	6.35
	P_Top	42.65	13.81	118.91	9.36	243.4	6.24
	P_HypTest	46.86	13.40	196.71	7.17	521.58	2.94
	P_Bayes	43.48	13.72	79.27	11.89	105.38	9.88
SemiSoft	S_Top	45.76	13.50	107.26	9.80	217.90	6.73
	P_Top	65.29	11.96	222.71	6.63	487.15	3.23